New supramolecular motifs for colloidal assembly

van Geffen, R.A.M.

Award date:
2015

New supramolecular motifs for colloidal assembly

Graduation report of

R.A.M. van Geffen

Molecular Engineering Master Program

Eindhoven University of Technology

New supramolecular motifs for colloidal assembly

Graduation report of
Rob Adrianus Maria van Geffen

Supervisors:
I. de Feijter MSc
Dr. J.A. Berrocal
Dr. Ir. I.K. Voets
Dr. Ir. A.R.A. Palmans

Supervising Professor:
Prof. Dr. E.W. Meijer

Advising Committee:
Dr. M.G. Debije

Eindhoven, February 2015

Laboratory of Macromolecular and Organic Chemistry
Department of Chemical Engineering and Chemistry
Eindhoven University of Technology

Summary

Supramolecular moieties are often used in systems to give function to materials. Nature has inspired mankind to create more dynamic and ordered systems, mimicking those present in cells and materials of natural origin. Making use of binding motifs that organize in a regular fashion, it is possible to obtain molecules that self-assemble in a desired fashion resulting in favorable material properties.

An often used binding moiety is the benzene-1,3,5-tricarboxamide (BTA) motif that organizes in a regular fashion by π-π interactions and the formation of hydrogen bonds between consecutive units. In this way, a helical columnar aggregate is created in certain solvents. However, more control over the formation of these helical columns is desired. In this way, we can enhance the ability to direct the assembly and dissociation to greater extent, thereby enabling the tuning of material properties in a desired fashion.

In this project, light responsive BTAs were synthesized and evaluated. These BTAs are intended to switch between two conformations due to the presence of an azobenzene unit in the molecule. As a result of the conformational change, the molecule loses the possibility to form hydrogen bonds between the consecutive units. This conformational change can be induced by irradiation of the azo-bond with light, which leads to isomerization. An adjusted, asymmetric, light responsive BTA was designed in order to get better solubility of the BTA and to enable coupling of the BTA to colloids.

First, a symmetrically substituted, light responsive BTA was synthesized and characterized. Then, the asymmetric, adjusted variant was synthesized. In this research a few synthetic routes were evaluated to investigate the feasibility of these synthetic routes to be able to synthesize the asymmetric light responsive BTA.

The assembly behaviour of the light responsive BTAs were studied using varying techniques including ultraviolet-visible (UV-Vis) spectroscopy, dynamic light scattering (DLS) and circular dichroism (CD) spectroscopy in various solvents. Self-assembly of the symmetric BTA occurred in a mixture of 50% dimethyl sulfoxide−water. In contrast, self-assembly of the asymmetric BTA occurred in toluene. The formation of hydrogen bonds between consecutive asymmetric light responsive BTAs was confirmed using infrared (IR) spectroscopy. Solid state analysis of this BTA, making use of polarized optical microscopy (POM) and wide angle X-ray scattering (WAXS), revealed that this BTA is packed in a hexagonal columnar fashion as expected for BTAs.

The isomerization reaction, upon irradiation with UV-light, of the symmetric and asymmetric BTA was investigated using UV-Vis spectroscopy. These measurements showed that the isomerization does take place upon irradiation with UV and visible light from *trans* to *cis* and vice versa.

Furthermore, the orthogonality of the self-assembly of the BTA and a core extended BTA were examined in order to determine whether it is possible to use these two binding motifs in one system. Using CD spectroscopy, it was determined that these motifs self-assemble in an orthogonal fashion and have no significant influence on each other's behaviour. Therefore, it is possible to use these binding motifs in one system and control the self-assembly of them independent of each other.

Table of Contents

Chapter 1: Introduction

1.1 Colloids

Colloids can be considered as the building blocks of materials in the same way as atoms are considered to be the building blocks of molecules.[1] Research on colloids has received a great deal of interest due to the possibility to control the features (size, shape) of these building blocks, as well as their assembly, which results in interesting properties such as the photonic properties of colloidal crystals. In order to have control over the material properties, it is necessary to obtain colloids with specific shapes, which have the capability to bind directionally in a material. Also, control over long- and short-range interactions between colloids is needed. Ultimately, the aim is to precisely place and orient these building blocks in materials.

The interactions that can play a role in colloidal assembly are:[2]

- Electrostatic forces
- Dipole forces
- Magnetic interactions
- Van der Waals forces
- Entropic forces (e.g. depletion force)
- Molecular surface forces (e.g. hydrogen bonding, donor-acceptor interactions and covalent bonds)

Only some of these interactions can be influenced using external triggers. Therefore, not all of these interactions are suitable to gain control over colloidal assembly. In this research, molecular surface forces will be used to influence the assembly.

By careful tuning these interactions to (direct) the assembly of colloids, a lot of different materials and clusters in solution have already been prepared.[1] A good example is that of colloidal gold particles of two different sizes that were decorated with complementary DNA strands.[3] When certain diameter ratios were used, this resulted in structures build up as an ionic crystal. In this example the coordination number and symmetry were controlled by varying the size ratios of the used gold particles (see Figure 1.1 a and b). As can be seen in the figures, the obtained structures are very similar to those of an ionic crystal (see Figure 1.1 c).

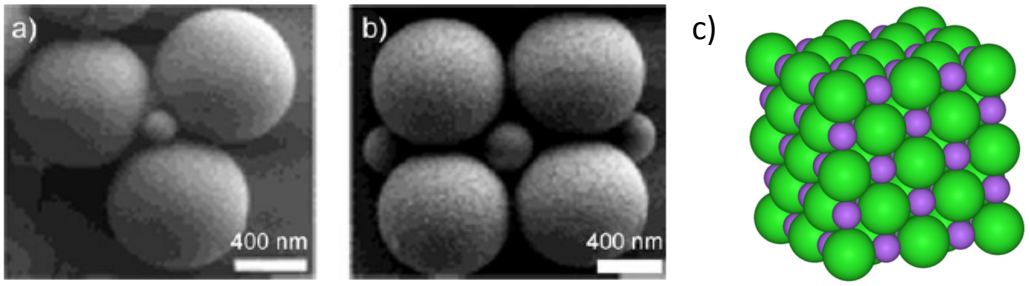

Figure 1.1: a) and b) are scanning electron microscopy (SEM) pictures of DNA based assemblies of binary colloids, wherein the small particles were surrounded by larger colloids depending on the size ratios, resulting in a ionic crystal like structure as depicted in c).[2]

Another example of colloidal assembly is shown in the self-assembly of silver nanocubes.[4] In their research cubic-shaped colloidal particles were prepared. It was possible to functionalize specific faces of the cubes with either hydrophobic (octadecanethiol) or hydrophilic (mercaptohexadecanoic acid) self-assembled monolayers (SAMs). By introducing these hydrophobic or hydrophilic monolayers on the colloidal particles, these sides tend to self-assemble due to hydrophobic driving forces. The number of faces that were functionalized with hydrophilic and hydrophobic SAMs was varied. This resulted in different structures when the particles assembled in water to reduce their hydrophobic interface that was exposed to water (see Figure 1.2). In this way they achieved directional assembly of these silver nanocubes.

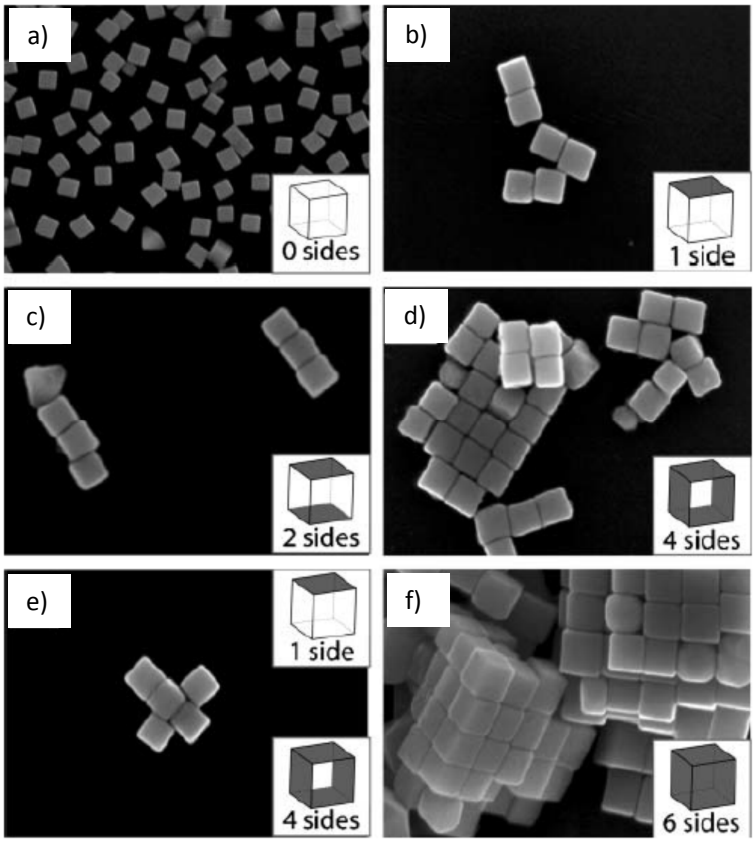

Figure 1.2: SEM images of Ag cubes (97 ± 6 nm) that were functionalized on 0 to 6 sides, resulting in different structures depending on which sides were modified.[4]

When it is possible to control the interactions between colloids to a greater extent it gives the opportunity to gain more control over the material properties by, for example, influencing the interaction stength between the colloids. In this way, it becomes possible to create a material that responds to its environment or applied triggers in a desired way. Therefore, it would be of great interest to have more interactions such as surface grafted supramolecular moieties that can be influenced and controlled in a precise way, thereby permitting to control the material properties to a greater extent.

1.2 Supramolecular motifs

The complex and highly functional structures present in nature have inspired many scientists to mimic this complexity. The ultimate aim is to be able to control molecular systems like nature is able to. Self-assembly and the interactions responsible for these have been extensively explored since the 19th century.[5] Self-assembling molecules using a wide variety of supramolecular interactions, such as hydrogen bonding, ion-ion and π-π interactions and hydrophobic effects, are well known and studied. Making use of these motifs that organize in a regular pattern, it is possible to obtain molecules that recognize these patterns and self-assemble in a desired fashion resulting in favorable material properties.

In our group benzene-1,3,5-tricarboxamides (BTAs) and 2-ureido-4-pyrimidinones (UPys) have been investigated extensively as supramolecular binding motifs.[6-12] The UPys are thoroughly investigated for their ability to form dimers at room temperature (see Figure 1.3). Making use of these UPy derivatives it is possible to form stable polymeric chains and networks.[13, 14] The UPy moiety is used in the formation of biomedical materials, organogels and self-healing polymers due to its dynamic and strong dimerization behaviour.[15-18] The BTAs will be discussed in more detail in paragraph 1.3.

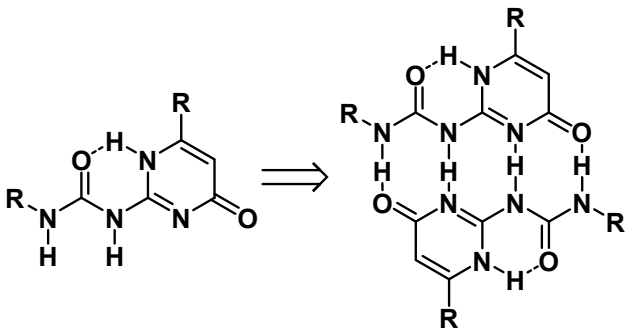

Figure 1.3: General structure of the UPy moiety (left) and dimerized form of the UPy moieties (right).

1.3 Benzene-1,3,5-tricarboxamides

Benzene-1,3,5-tricarboxamides were reported for the first time by Curtis in 1915, and consist of a benzene core and amides connected at the 1, 3 and 5 position (see Figure 1.4).[19]

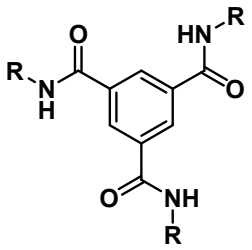

Figure 1.4: General chemical structure of a BTA.

Due to their easy accessibility and interesting properties, their self-assembly and supramolecular chemistry has been studied extensively, in this and other groups.[8, 9, 20] It was shown that BTAs form helical columnar stacks through threefold hydrogen bonding, between the amides of consecutive BTAs, and π-π interactions between them, both in solid state and dissolved in apolar organic solvents such as heptane and methylcyclohexane (see Figure 1.5).[6, 7] In methanol and chloroform these aggregates are not observed, and the BTAs are molecularly dissolved in these solvents.[21]

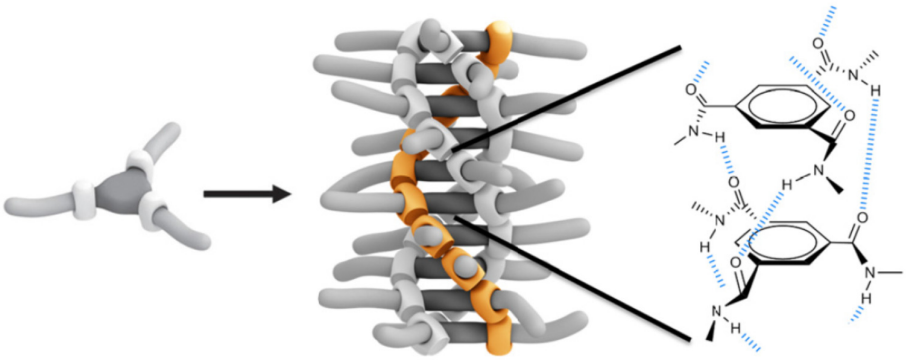

Figure 1.5: Schematic representation of BTA self-assembly into helical columns via threefold hydrogen bonding and π-π interactions.

Chiral BTAs give typical ultraviolet (UV) and circular dichroism (CD) spectra as shown in Figure 1.6. At room temperature, a Cotton effect is observed around 220 nm.[21] At higher temperatures, no CD signal is observed anymore, as a result of the dynamic behaviour of the intermolecular hydrogen bonding at these temperatures, the BTAs are molecularly dissolved and therefore no CD signal is observed. The Cotton effect is the result of the packing of the molecules due to the hydrogen bonding, placing the dipoles of the molecules in an arranged way on top of each other. The UV spectrum also is affected by the loss of the hydrogen bonding at higher temperatures (see Figure 1.6).

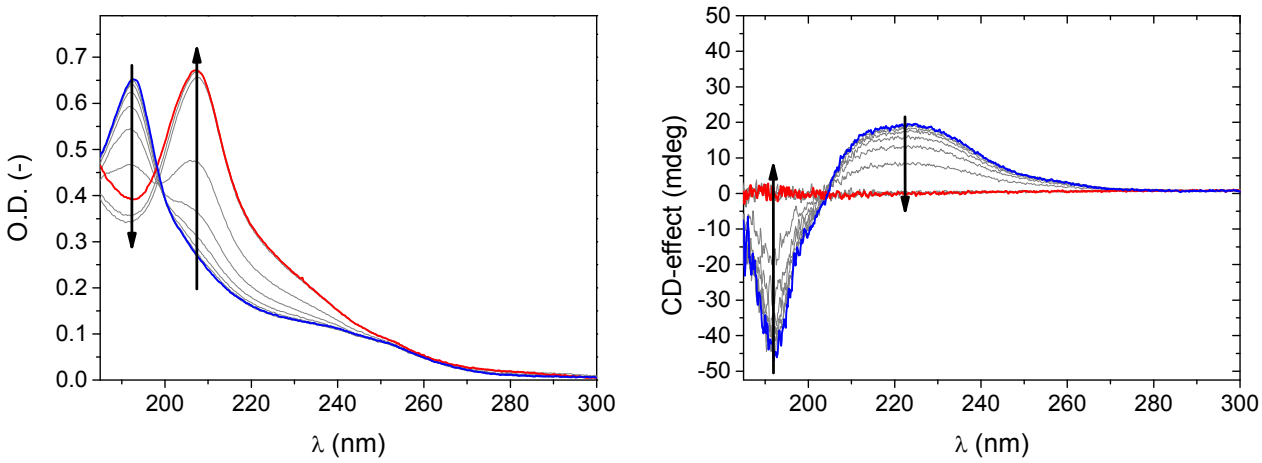

Figure 1.6: Absorption (left) and CD (right) spectra of a BTA in heptane at low temperature (blue) and high temperature (red).[22]

By introducing a protecting group on the BTA, which prevents hydrogen bonding between the BTAs, self-assembly can be prevented. The protection group that was used in our group is *o*-nitrobenzyl that is photolabile and therefore can be cleaved of using light (see Figure 1.7).[23] In this way, the self-assembly can be controlled by the deprotection time of the BTAs.

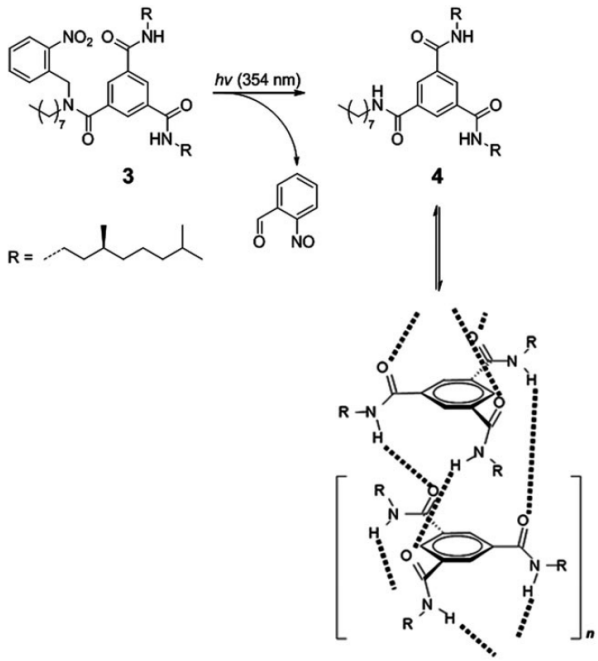

Figure 1.7: Representation of a protected BTA upon deprotection with UV-light the molecule becomes able to form hydrogen-bonds and self-assemble.[23]

1.4 Colloid assembly via external triggers

Fusion of self-assembling supramolecular motifs such as BTAs, with building blocks such as colloids, gives the opportunity to create dynamic materials that respond to external triggers. Many supramolecular bonds dissociate at high temperatures, this also applies to BTAs. From a practical

point of view, this is disadvantageous because the system is only dissociated as long as the sample is heated. Therefore it is of interest to develop a system that can be turned on and off by a simple external trigger, such as light, at room temperature. In this group, I. de Feijter *et al.* grafted benzene-1,3,5-tricarboxamide protected with *o*-nitrobenzyl groups to the surface of silica beads. The used BTA is known to self-assemble in an apolar solvent,[7] hence activation of the BTAs by cleaving off of the protecting group with light leads to self-assembly. In this way association of the silica beads can be induced upon UV irradiation (see Figure 1.8).[24] However, this is not a reversible process.

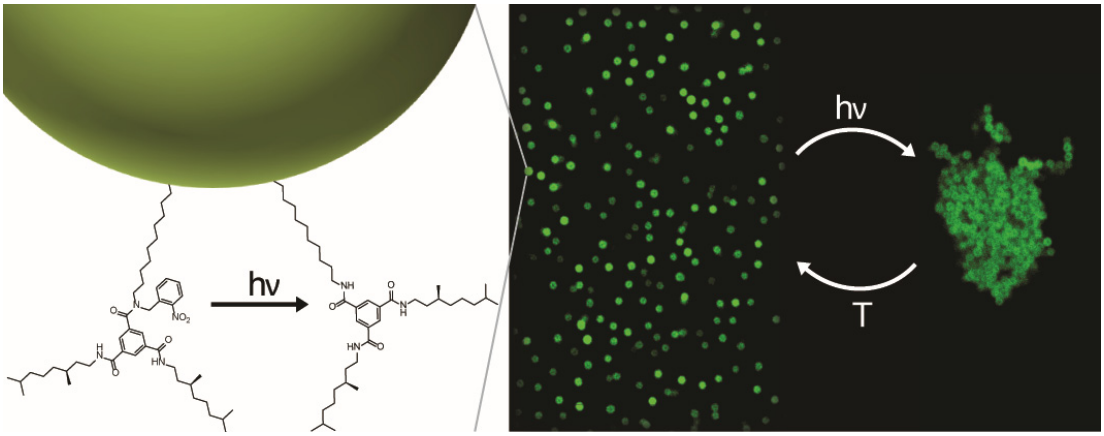

Figure 1.8: Left) Schematic representation of surface grafted benzene-1,3,5-tricarboxamide (BTA). Right) Fluorescence microscopy image of fluorescently labeled silica bead with the binding motifs grafted onto the surface, and assembly and dissociation by external triggers.

In order to create a fully reversible system, a supramolecular moiety has to be developed that can be reversibly controlled via light in order to activate and disrupt aggregation of the molecules. Therefore a molecule is required that undergoes a conformational change due to an external light trigger in order to disrupt the aggregation.

1.5 Azobenzene(-derivatives)

Azobenzenes exist in both the *trans* and *cis* conformation, and the isomerization from *trans* to *cis* state occurs due to irradiation with ultraviolet-light,[25,26] electrostatic stimulation[27] or mechanical stress.[28] However, *cis* to *trans* isomerization occurs spontaneously due to thermal relaxation because of the better thermodynamic stability of the *trans* conformation.[26]

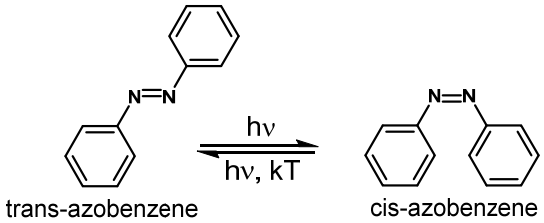

Figure 1.9: Isomerization of azobenzene.

The quantum yield and isomerization mechanism is influenced by factors such as irradiation wavelength,[29] solvent properties,[30] substituents on the phenyl rings,[31] temperature[32] and pressure.[33] The photo-isomerization from the *trans* to the *cis* conformation can be followed making use of ultraviolet-visible spectroscopy. When the azo-compound is irradiated with UV light, the peak belonging to the molecule *trans* conformation decreases in intensity and the peak at higher wavelength that corresponds to the *cis* conformation increases (see Figure 1.10). These peaks can shift due to the substituents on the azobenzene by presence of electron donating or withdrawing groups.

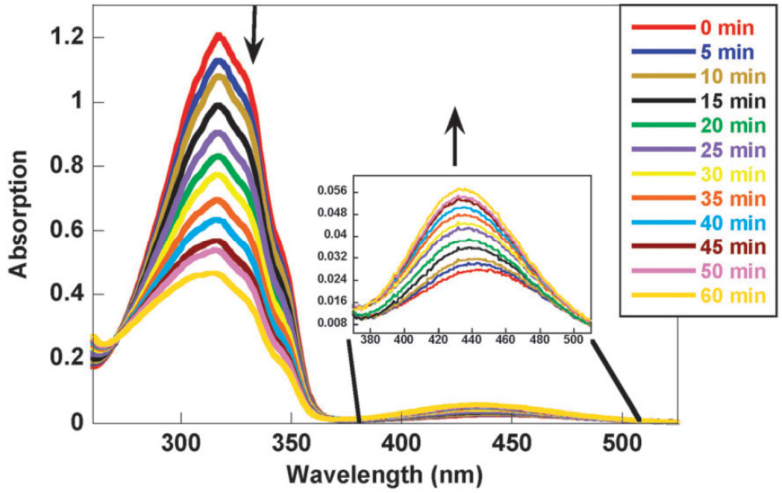

Figure 1.10: The absorption spectrum of azobenzene (AB) upon irradiation with UV light (316 nm).[34]

Azobenzene derivatives have been used in studies to make self-erasable and rewritable materials.[35] Materials with silver nanoparticles with an azobenzene derivative have been exposed to UV light using a photomask in order to obtain an image. The self-erasing occurred during 9 hours in daylight but using intense visible light the image was erased in 60 seconds. As a result the material is able to switch between images and an erased state.

The azobenzene moiety coupled to the BTA unit was recently examined by Huang and Kim as a photo-responsive surfactant for gold nanoparticles.[36] The conformational change due to the *trans–cis* isomerization induced assembly of the gold nanoparticles. This leads to the formation of blackberry-like nanoparticles and multilayered plates depending on the used irradiation wavelength during the growth (see Figures 1.11 and 1.12).

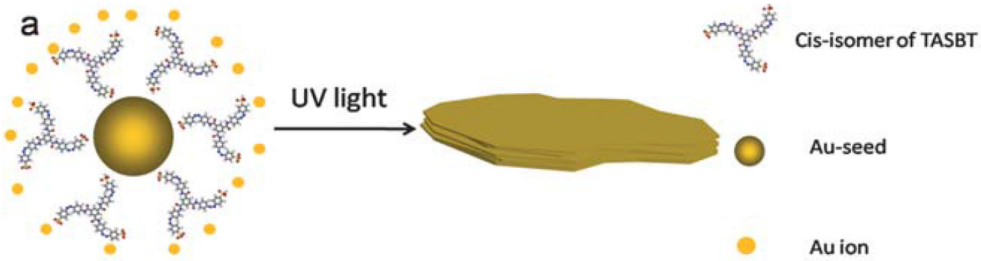

Figure 1.11: a) Schematic representation of the light responsive surfactant molecule and the growth of the gold seeds under influence of irradiation.[36]

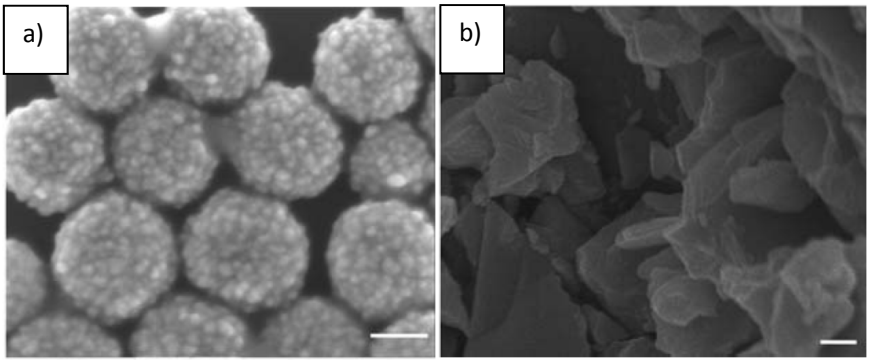

Figure 1.12: a) and b) SEM images of the gold nanoparticles under irradiation with visible-light a) and UV-light b). The scale bar represents 100 nm in a) and 200 nm in b).[36]

The isomerization property of the azo-bond was recently also used in a BTA by Lee *et al.*, making use of the conformational change that occurs upon this isomerization. Their research showed that disruption, of the formed aggregates, occurs in certain solvents upon irradiation of the molecules with UV-light, due to the conformational change.[37] The irradiation of the azobenzene derived BTA with UV-light resulted, in the disappearance of the formed aggregates. While irradiating the samples then with visible-light resulted in reformation of long, fibrillar aggregates (see Figure 1.13). It was shown that this cycle could be repeated multiple times without degradation of the material.

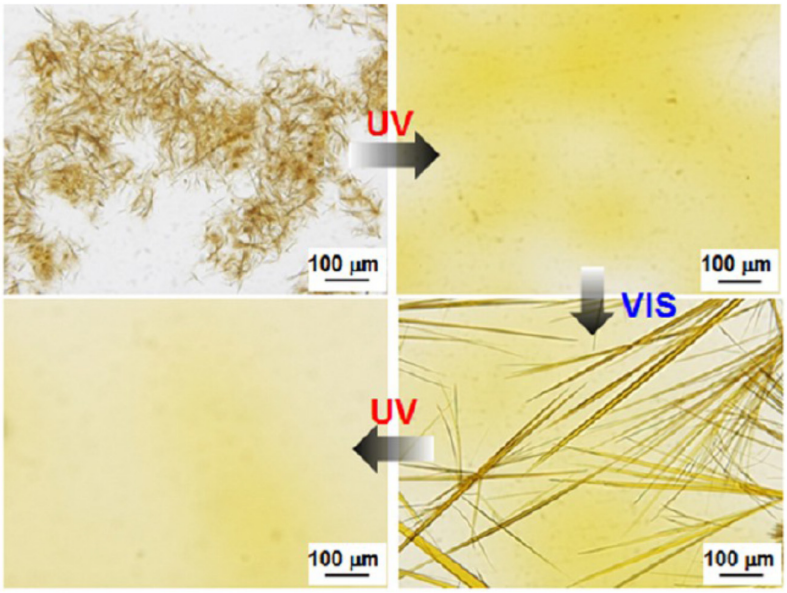

Figure 1.13: Optical microscopy pictures of the azo-BTA in 50% DMSO – H_2O upon irradiation with UV and visible-light.[37]

Since the photo-isomerization is reversible and thus the aggregation of the BTAs is switched on and off upon the isomerization, this molecule is useful to switch between an associated and dissociated state making use of light as a simple external trigger. In order to enable the coupling of the BTA to silica beads its structure first has to be modified. In this way, it is possible to improve the system

shown before, in which a light cleavable BTA was used. Making use of the conformational change that occurs due to the isomerization, using this BTA disaggregation could be achieved by light of a different wavelength instead of constant heating of the sample.

1.6 Aim of this project

The aim of this project is to develop the next generation of supramolecular colloids by surface-grafting BTAs onto silica beads that reversibly associate and dissociate upon UV-Vis irradiation at room temperature. The first step is to synthesize and characterize BTA **1** (see Figure 1.14), tris(4-((*E*)-phenyldiazenyl)phenyl)benzene-1,3,5-tricarboxamide which, according to literature, participates in light driven, reversible *cis-trans* photoisomerization reactions as discussed above.[37] Secondly, we will verify if these BTAs stack and dissociate upon irradiation by light of different wavelengths. Subsequently we will test whether they can be used as a binding moiety to orchestrate the assembly of silica colloids. Therefore BTA **2** was designed in such a way that it can be grafted onto the surface of silica beads. Furthermore, chiral centra were introduced (see Figure 1.14) to allow the use of CD-spectroscopy for monitoring the self-assembly behaviour. BTA **2** will be synthesized, characterized and its self-assembly studied in solution. Finally we will determine which grafting method can be used to attach BTA **2** onto the silica colloids, characterize these supramolecular light-switchable colloids and probe colloidal assembly.

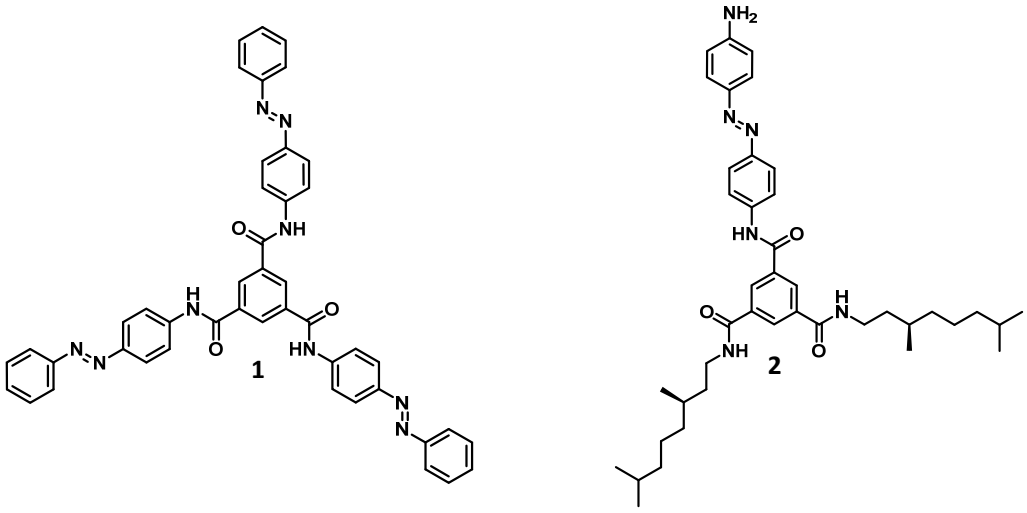

Figure 1.14: 1 Structure of the light sensitive azobenzene BTA. **2** Structure of modified BTA for surface grafting.

The synthesis and characterization of both BTAs **1** and **2** and the BTA coupled to the colloids will be discussed in chapter 2. The light-driven isomerization reaction and the effect of switching on the assembly will be discussed in chapter 3. Also the possibility to use two different BTAs, namely the BTA that is studied extensively in our group (see above) and a core extended variant (oligo(phenylene ethynylene) tricarboximides) or OPE-TA, is examined in chapter 4. The use of two supramolecular moieties in one system gives the opportunity to have a better control over the material properties, in order to gain this better control the used moieties should not influence each other.

1.7 References

1. F. Li, D. P. Josephson and A. Stein, *Angew. Chem. Int. Ed.*, 2011, **50**, 360-388.
2. K. J. M. Bishop, C. E. Wilmer, S. Soh and B. A. Grzybowski, *Small*, 2009, **5**, 1600-1630.
3. C. M. Soto, A. Srinivasan and B. R. Ratna, *J. Am. Chem. Soc.*, 2002, **124**, 8508-8509.
4. M. Rycenga, J. M. McLellan and Y. Xia, *Adv. Mater.*, 2008, **20**, 2416-2420.
5. J.-M. Lehn, *Angew. Chem. Int. Ed.*, 1988, **27**, 89-112.
6. P. J. M. Stals, M. M. J. Smulders, R. Martín-Rapún, A. R. A. Palmans and E. W. Meijer, *Chem.-Eur. J.*, 2009, **15**, 2071-2080.
7. S. Cantekin, T. F. A. de Greef and A. R. A. Palmans, *Chem. Soc. Rev.*, 2012, **41**, 6125-6137.
8. T. F. A. de Greef, M. M. L. Nieuwenhuizen, P. J. M. Stals, C. F. C. Fitie, A. R. A. Palmans, R. P. Sijbesma and E. W. Meijer, *Chem. Commun.*, 2008, 4306-4308.
9. P. J. M. Stals, J. F. Haveman, A. R. A. Palmans and A. P. H. J. Schenning, *J. Chem. Educ.*, 2009, **86**, 230.
10. E. J. Foster, E. B. Berda and E. W. Meijer, *J. Am. Chem. Soc.*, 2009, **131**, 6964-6966.
11. E. B. Berda, E. J. Foster and E. W. Meijer, *Macromolecules*, 2010, **43**, 1430-1437.
12. E. J. Foster, E. B. Berda and E. W. Meijer, *J. Polym. Sci., Part A: Polym. Chem.*, 2011, **49**, 118-126.
13. R. P. Sijbesma, F. H. Beijer, L. Brunsveld, B. J. B. Folmer, J. H. K. K. Hirschberg, R. F. M. Lange, J. K. L. Lowe and E. W. Meijer, *Science*, 1997, **278**, 1601-1604.
14. F. H. Beijer, R. P. Sijbesma, H. Kooijman, A. L. Spek and E. W. Meijer, *J. Am. Chem. Soc.*, 1998, **120**, 6761-6769.
15. D. J. M. van Beek, A. J. H. Spiering, G. W. M. Peters, K. te Nijenhuis and R. P. Sijbesma, *Macromolecules*, 2007, **40**, 8464-8475.
16. J.-L. Wietor, A. Dimopoulos, L. E. Govaert, R. A. T. M. van Benthem, G. de With and R. P. Sijbesma, *Macromolecules*, 2009, **42**, 6640-6646.
17. P. Y. W. Dankers, P. J. H. M. Adams, D. W. P. M. Löwik, J. C. M. van Hest and E. W. Meijer, *Eur. J. Org. Chem.*, 2007, **2007**, 3622-3632.
18. P. Y. W. Dankers, E. N. M. van Leeuwen, G. M. L. van Gemert, A. J. H. Spiering, M. C. Harmsen, L. A. Brouwer, H. M. Janssen, A. W. Bosman, M. J. A. van Luyn and E. W. Meijer, *Biomaterials*, 2006, **27**, 5490-5501.
19. T. Curtius, *J. Prakt. Chem.*, 1915, **91**, 39.
20. K. Matsuura, K. Murasato and N. Kimizuka, *J. Am. Chem. Soc.*, 2005, **127**, 10148-10149.
21. L. Brunsveld, A. P. H. J. Schenning, M. A. C. Broeren, H. M. Janssen, J. A. J. M. Vekemans and E. W. Meijer, *Chem. Lett.*, 2000, **29**, 292-293.
22. M. M. J. Smulders, A. P. H. J. Schenning and E. W. Meijer, *J. Am. Chem. Soc.*, 2007, **130**, 606-611.
23. T. Mes, R. van der Weegen, A. R. A. Palmans and E. W. Meijer, *Angew. Chem. Int. Ed.*, 2011, **50**, 5085-5089.
24. I. de Feijter, L. Albertazzi, E. W. Meijer, A. R. A. Palmans and I. K. Voets, *Langmuir*, 2014.
25. H. Knoll, *CRC Handbook of Organic Photochemistry and Photobiology*, 2004, **2nd edn**, 89/81–89/16.
26. H. Rau and E. Lueddecke, *J. Am. Chem. Soc.*, 1982, **104**, 1616-1620.
27. X. Tong, M. Pelletier, A. Lasia and Y. Zhao, *Angew. Chem. Int. Ed.*, 2008, **47**, 3596-3599.
28. R. Turansky, M. Konopka, N. L. Doltsinis, I. Stich and D. Marx, *Phys. Chem. Chem. Phys.*, 2010, **12**, 13922-13932.
29. L. Wang, W. Xu, C. Yi and X. Wang, *J. Mol. Graphics Modell.*, 2009, **27**, 792-796.
30. P. Bortolus and S. Monti, *J. Phys. Chem.*, 1979, **83**, 648-652.
31. H. Rau, *Photoreact. Org. Thin Films*, 2002, 3-47.
32. E. Fischer, *J. Am. Chem. Soc.*, 1960, **82**, 3249-3252.
33. T. Asano, T. Yano and T. Okada, *J. Am. Chem. Soc.*, 1982, **104**, 4900-4904.
34. H. M. D. Bandara and S. C. Burdette, *Chem. Soc. Rev.*, 2012, **41**, 1809-1825.

35. R. Klajn, P. J. Wesson, K. J. M. Bishop and B. A. Grzybowski, *Angew. Chem. Int. Ed.*, 2009, **48**, 7035-7039.
36. Y. Huang and D.-H. Kim, *Nanoscale*, 2012, **4**, 6312-6317.
37. S. Lee, S. Oh, J. Lee, Y. Malpani, Y.-S. Jung, B. Kang, J. Y. Lee, K. Ozasa, T. Isoshima, S. Y. Lee, M. Hara, D. Hashizume and J.-M. Kim, *Langmuir*, 2013, **29**, 5869-5877.

Chapter 2: Synthesis and characterization of BTA derivatives

2.1 Introduction

To develop the next generation of supramolecular colloids by surface-grafting of BTAs that reversibly associate and dissociate upon UV-Vis irradiation at room temperature onto silica beads, a few steps had to be taken. The first step was to synthesize and characterize BTA **1** (see Figure 2.1) to further study its behaviour upon switching in dilute conditions.[1] The advantage of this BTA is that it is symmetric, so a symmetric precursor can be used. Secondly, BTA **2** was designed such that it could be grafted onto the surface of silica beads. Furthermore, the solubility was enhanced in this molecule by using only one azo-compound and two dihydrocitronellyl molecules as side chains. Additionally, chirality was introduced (see Figure 2.1) making it possible to use circular dichroism (CD) spectroscopy to investigate the self-assembly of the moieties. This molecule is asymmetric and therefore an asymmetric precursor had to be used, making the synthesis of BTA **2** more difficult compared to **1**. Roosma *et al*. reported a synthetic strategy to obtain desymmetrised BTAs in three additional steps.[2]

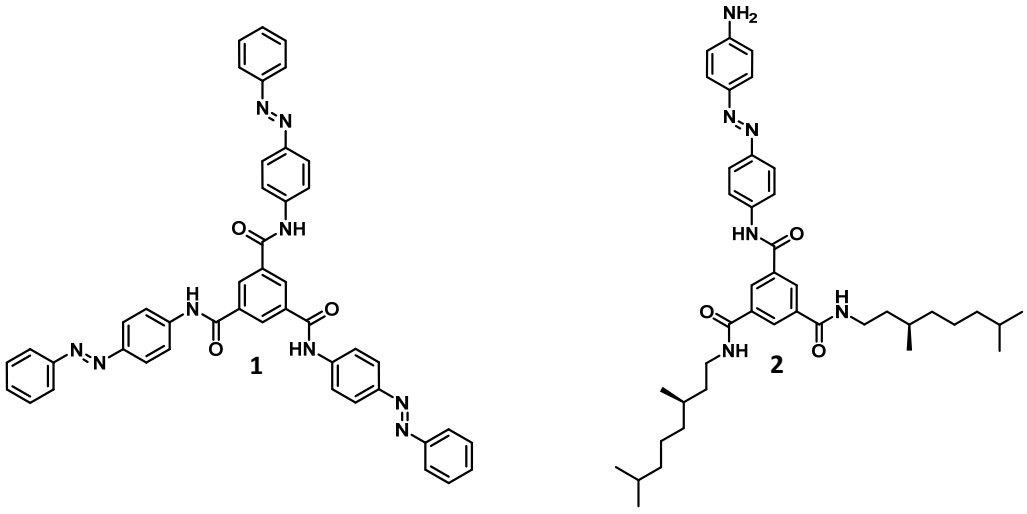

Figure 2.1: Structure of the light sensitive azobenzene BTA **1**. Structure of modified BTA **2** for surface grafting.

In this project, we start from a symmetric and an asymmetric BTA to synthesize **1** and **2**, respectively. The starting BTA that was used, which in case of BTA **2** was already desymmetrised making use of the strategy of Roosma *et al.*, was kindly provided by Jolanda Spiering. The synthesis of BTA **2** was not yet studied and therefore it was necessary to develop a synthesis route. To synthesize BTA **2**, a few routes were evaluated (see Scheme 2.1).

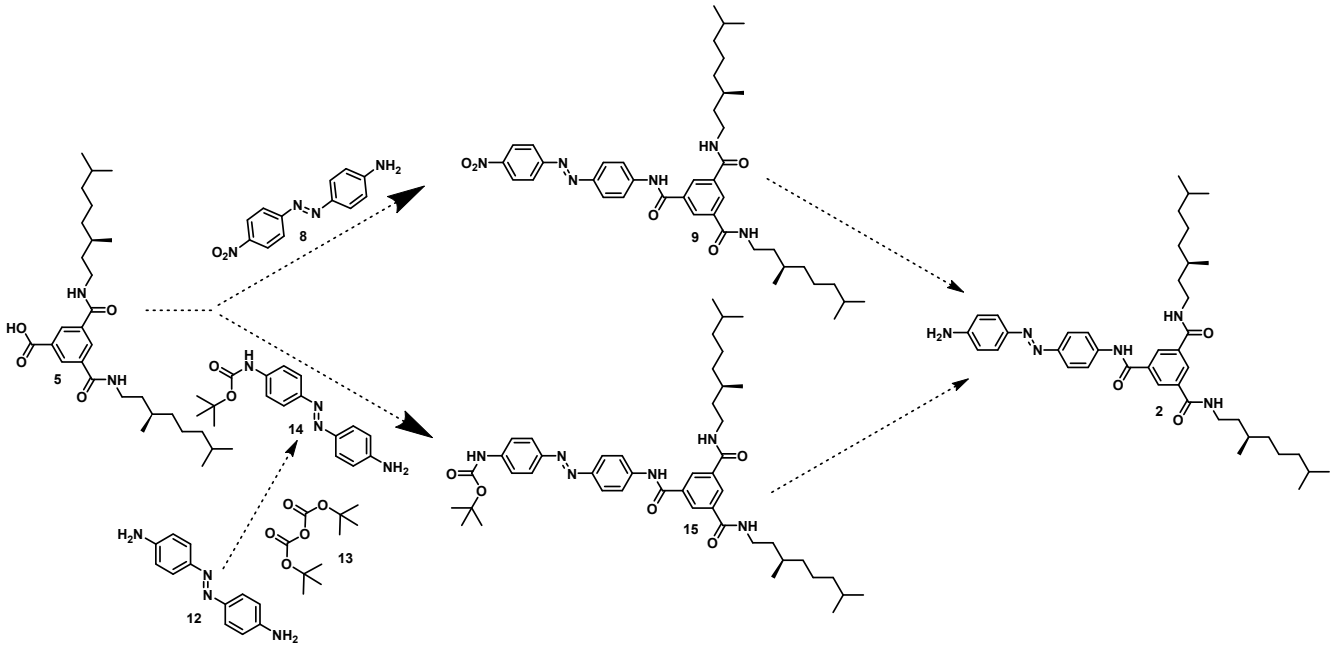

Scheme 2.1: Synthetic routes evaluated to obtain molecule **2**.

To make the BTA ready for grafting onto silica beads it had to be coupled to succinic anhydride. The resulting BTA was suitable for coupling to silica beads in order to test the clustering behaviour upon irradiation, to develop a system which can be controlled by light to turn the self-assembly on and off.

2.2 Synthesis and molecular characterization of a symmetric light responsive BTA

Synthesis of 4-phenylazoaniline functionalized BTA

BTA **1** was synthesized, following a procedure from literature[1] (see Scheme 2.2), by slow addition of 1,3,5-benzenetricarbonyl chloride (**3**) to 4-phenylazoaniline (**4**) in THF in presence of triethylamine. After 48 hours stirring at room temperature, the reaction mixture was concentrated *in vacuo* and precipitated from tetrahydrofuran (THF) in methanol, giving the product **1**. The presence of the product was confirmed by nuclear magnetic resonance (NMR), infrared spectroscopy (IR) and MALDI-ToF mass spectroscopy (MS), and the reaction had a yield of 42%.

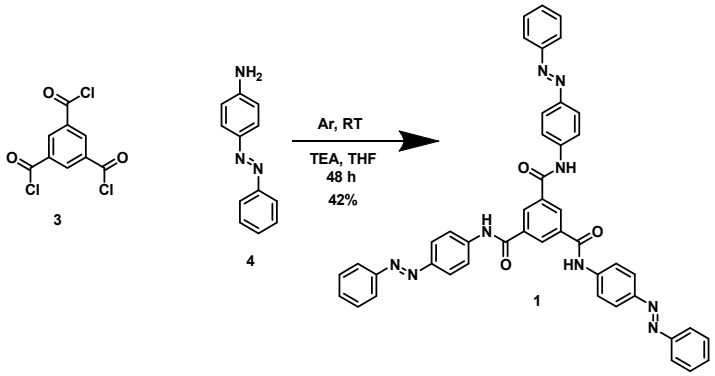

Scheme 2.2: Synthesis of BTA **1**.

Molecular characterization

Compound **1** was characterised using NMR, FT-IR and MALDI-TOF MS.

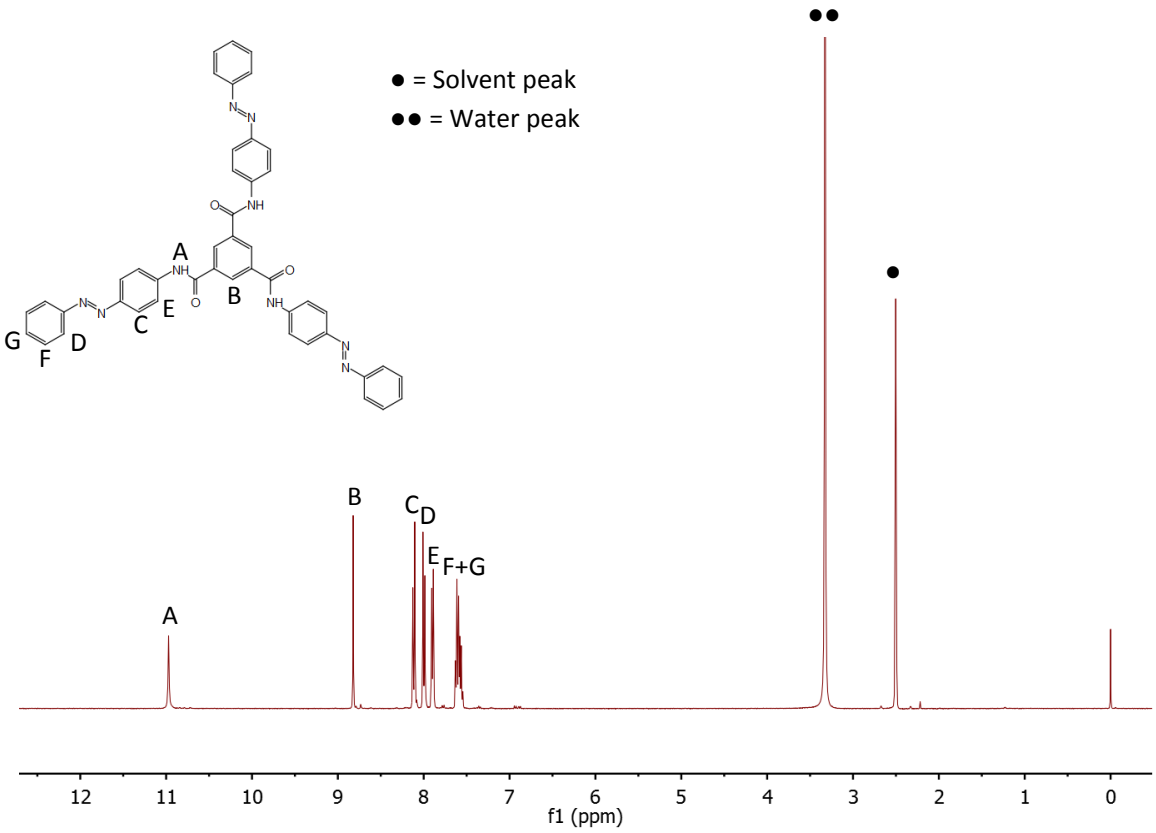

Figure 2.2: The ^{1}H-NMR spectrum of compound **1**.

The signals in the ^{1}H-NMR of compound **1** can all be assigned as shown in Figure 2.2, in accordance with literature.[1] The small peaks observed at 7.77, 7.35, 6.95 and 6.88 ppm correspond to the *cis* form of the molecule.

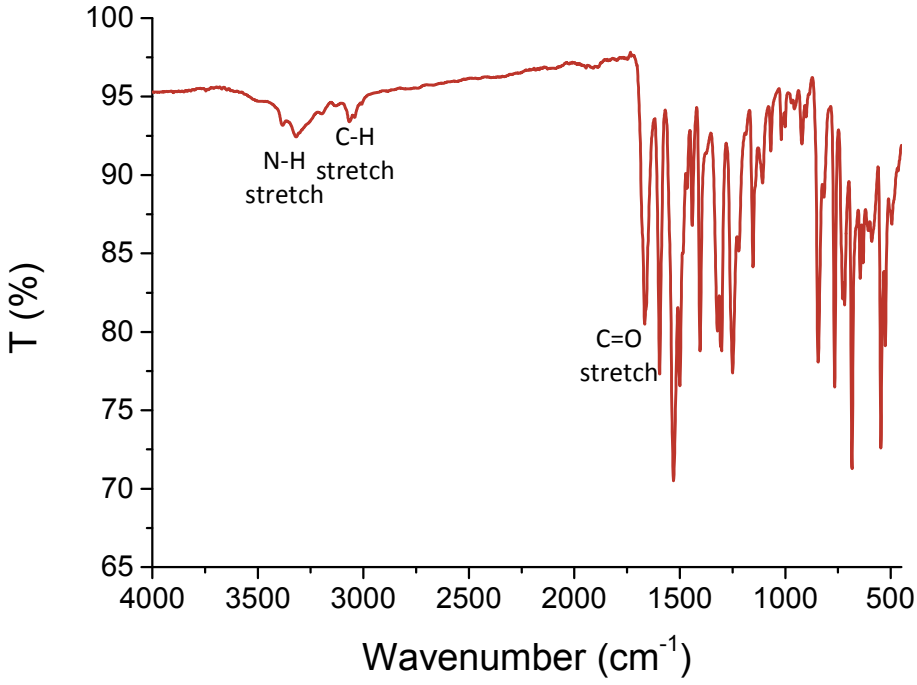

Figure 2.3: The IR spectrum of compound **1**.

The IR spectrum measured for compound **1** (see Figure 2.3) is identical to the one reported in literature, confirming the synthesis of BTA **1**.[1]

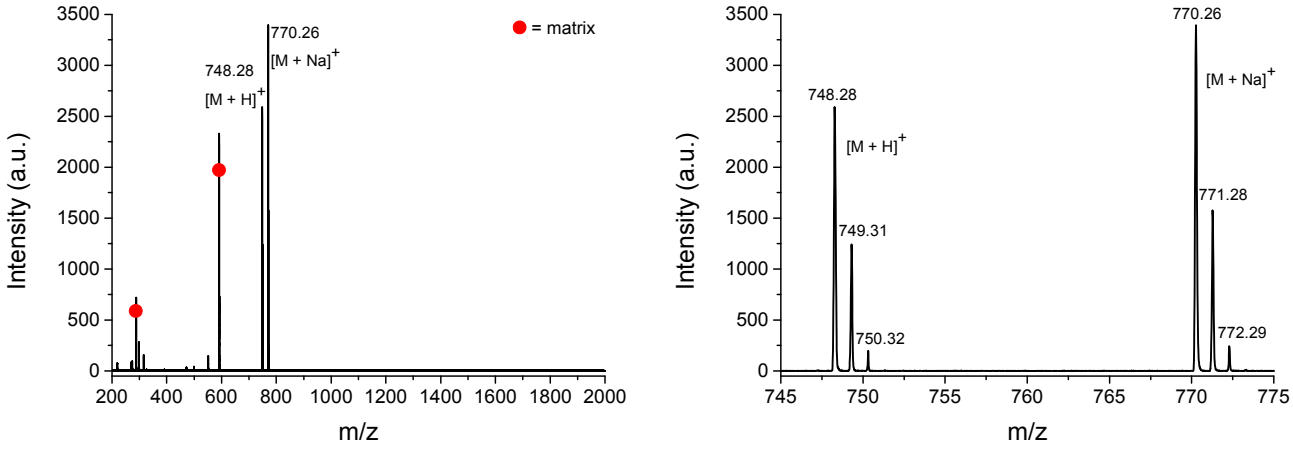

Figure 2.4: (Left) MALDI-ToF MS spectrum of compound **1**. (Right) zoom in of the spectrum showing the hydrogen and sodium adduct isotope peaks.

With MALDI-ToF MS the mass peaks of the product hydrogen and sodium adduct were found (see Figure 2.4). From the NMR, IR and MALDI-ToF MS results, a successful synthesis of BTA **1** can be concluded. Furthermore, the product of the synthesis is BTA **1** in good purity.

2.3 Synthesis and molecular characterization of a modified asymmetrically substituted BTA 2

Route 1: BOC-protection

The first approach towards synthesizing BTA **2** made use of the route shown in the bottom of Scheme 2.1. In this attempt to synthesize molecule **2**, diazoaniline was mono-protected with a tert-butoxycarbonyl-group (BOC-group) before coupling it to the BTA, to form the protected variant of molecule **2** and after cleaving of the BOC protection group the desired molecule was obtained. In order to use this route the mono-protected diazoaniline had to be synthesized. However, the purification of the statistic mixture obtained by this protection proved to be practically unattainable. Therefore, this method was abandoned.

Route 2: an asymmetric azo-compound

The second synthesis route that was developed, after the BOC- protection proved unsuccessful, made use of a commercially available asymmetric azo-compound instead of the symmetric one used in the first synthesis route (see Scheme 2.3). This asymmetric azo-compound will be coupled to the desymmetrised BTA **5**, kindly provided by Jolanda Spiering. However, before this route was used first a few test reactions were done to determine for example if an aromatic amine group is reactive enough to react with an acid chloride. Furthermore, a selective reduction had to be examined in order to reduce the nitro group into an amine without affecting the rest of the structure.

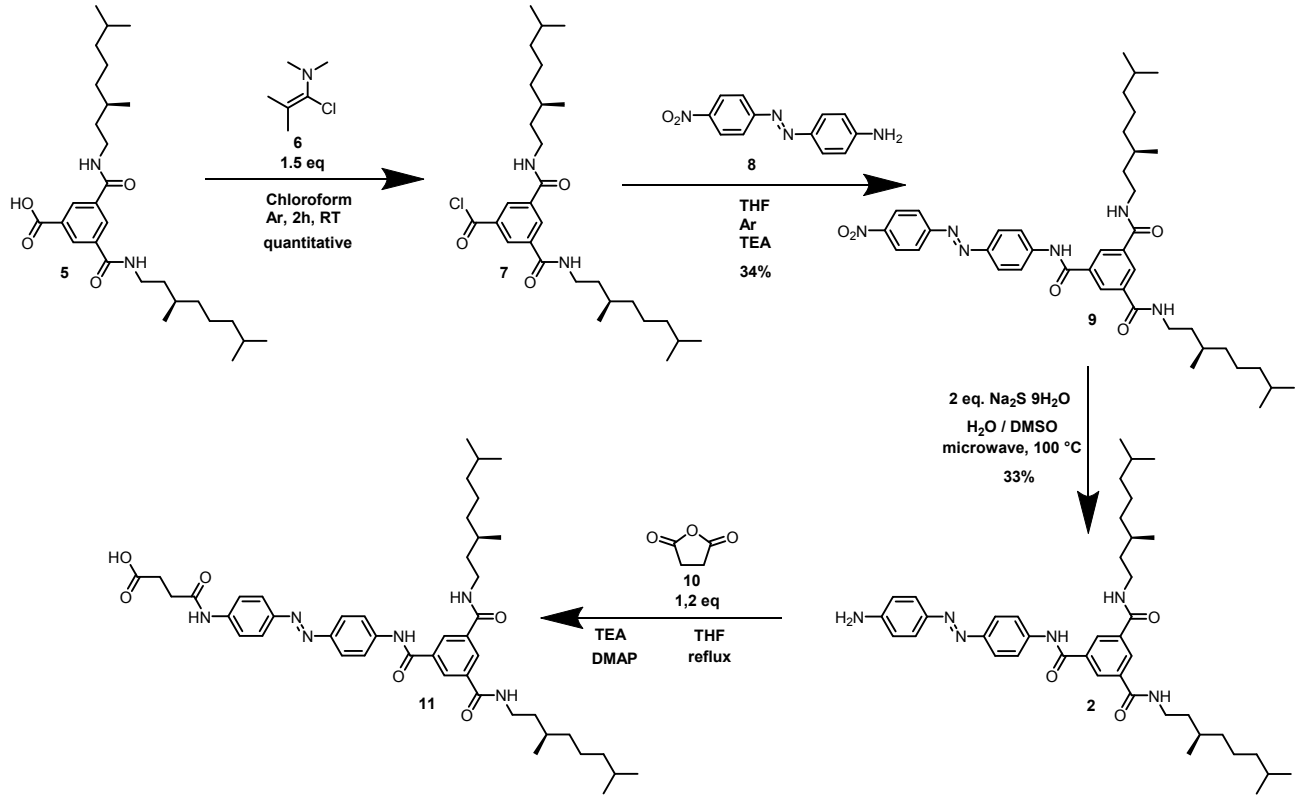

Scheme 2.3: Synthesis of BTA **2**, and coupling of **2** with succinic anhydride.

Test reaction; reactivity of an aromatic amine

In order to test the reactivity of an aromatic amine a test reaction was done to see whether an aromatic amine is reactive enough to react with an acid chloride. In this test reaction aniline was coupled to BTA **7** see Scheme 2.4. Compound **7** was obtained by the reaction between BTA **5** and Ghosez reagent **6**. The reaction was evaluated using IR, NMR and MALDI-ToF MS and showed that the synthesis was successful.

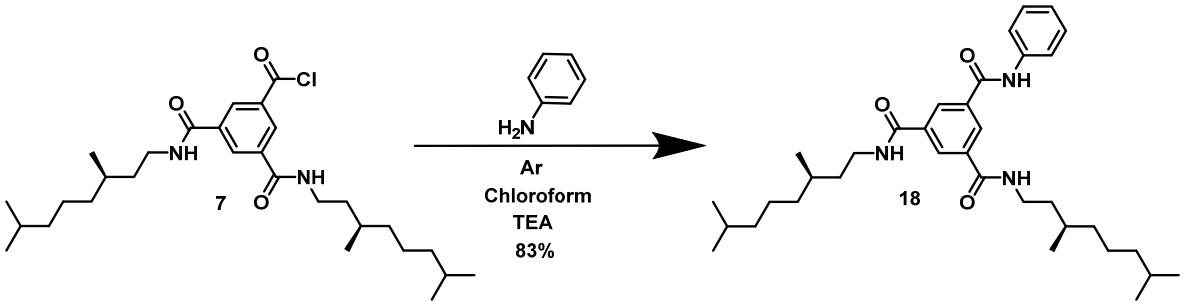

Scheme 2.4: Test reaction of a coupling of an aromatic amine to acid chloride

Selective reduction: the Zinnin reduction

After the coupling of the asymmetric azo-compound to the BTA the nitro group has to be selectively reduced. The used reaction is called the Zinnin reduction and was used instead of the more common reductions in order not to affect the azo bond of the molecule. The Zinnin reduction was discovered by Zinnin in 1842 in preparation of aniline from nitrobenzene.[3] The Zinnin reduction is used for the reduction of nitroarenes with a negative divalent sulphur such as sulphide or hydrosulphide. The reduction is used to produce aromatic amines when other methods are not possible due to unwanted side reactions or sensitivity of the compound as described earlier.

The mechanism of this reaction is not known. The stoichiometry of the reaction can be depicted, depending on the reducing species, as:

$$4\,ArNO_2 + 6\,S^{2-} + 7\,H_2O \longrightarrow 4\,ArNH_2 + 3\,S_2O_3^{2-} + 6\,OH^-$$

$$ArNO_2 + S_2^{2-} + H_2O \longrightarrow ArNH_2 + S_2O_3^{2-}$$

$$4\,ArNO_2 + 4\,HS^- + H_2O \longrightarrow 4\,ArNH_2 + 3\,S_2O_3^{2-}$$

Due to side reactions, this stoichiometry is not seen most of the cases and 1.6 mole equivalents up to 4 mole equivalents of the chosen reducing species are required to reduce one mole of nitro groups.

Some kinetic studies have been done for this reduction, these studies show:

- The disulphide ion is most effective reducing agent.
- The highest water concentration in the solvent mixture in which the compound is completely or partially dissolved gives the best kinetics for the reduction.
- An excess of alkali yields most of the reductant as sulphide or disulphide ion, giving better kinetics.
- An excess of the reductant should be used in order to not stop in an intermediate step of the reaction.

In order to test the Zinnin reduction 4-(4-nitrophenylazo)aniline (**8**) was reduced using this method. The reduction was tested in a mixture of 1,4-dioxane-ethanol with 2 equivalents of the sodium sulphide (see Scheme 2.5). However, no reaction was observed under reflux or in the microwave reactor trying many different reaction conditions. Only when the ethanol was exchanged for water, as recommended by literature, the reaction did occur. This already showed the importance of water for the mechanism. The presence of the product was confirmed with NMR and MALDI-ToF, showing that this selective reduction works and does not affect the azo-bond.

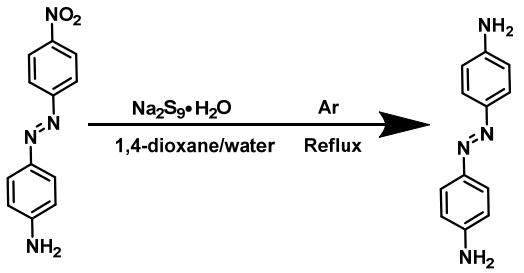

Scheme 2.5: Test reaction of the Zinnin reduction

In the experiments performed in this study making use of the Zinnin reduction it was observed that a dimethyl sulfoxide (DMSO)-water mixture was a better solvent choice compared to a THF-water mixture and the addition of triethylamine did not significantly change the reaction kinetics.

Synthesis of 4,4-azodianiline functionalized BTA

Having confirmed that the azo-compound should be able to couple with the BTA, and selective reduction of the nitro group is possible, the synthesis of BTA **2** was started. **1**-Chloro-*N*,*N*,-2-trimethyl-1-propenylamine (**6**) was added to BTA **5** in chloroform. After 2 hours stirring the reaction mixture was concentrated *in vacuo*. The residue was dried thoroughly using high vacuum. Full conversion to **7** was confirmed using infrared spectroscopy using the carbonyl signal of the acid/acid-chloride at 1704 cm^{-1} that shifts to 1763 cm^{-1}, as can be observed in Figure 2.5.

4-(4-Nitrophenylazo)aniline (**8**) was added to **7** and triethylamine in THF while the mixture was cooled in an ice-bath. After allowing the mixture to warm up the mixture was stirred 24 hours, before full conversion was confirmed by infrared spectroscopy (see Figure 2.5). The mixture was concentrated *in vacuo* and purified with column chromatography giving a reaction yield of 34% in BTA **9**.

Unfortunately it became evident after column chromatography that hydrolysis of the newly formed amide bond between **8** and **7** finds place during this purification, probably due to the light acidity of the silica column. The fact that the amide bond is hydrolysed so easily shows that this amide bond is not very stable and this has to be taken into account in further research. For this reason it was necessary to come up with a new purification method. Since **8** is better soluble in diethyl ether compared to product **9,** trituration was used to purify the product resulting in a yield of 52%.

The conversion of the reactions going from **5** to **7** and from **7** to **9** were followed looking at the carbonyl peak with infrared (IR) spectroscopy. The carbonyl peak of **5** corresponding to the acid (1704 cm^{-1}) shifts during the reaction to the left when the acid chloride is formed (1763 cm^{-1}). The

formed carbonyl peak disappears again when the azo compound is coupled to **7** due to the amide that forms at cost of the acid chloride. A small amount of the acid chloride is still left, before purification, as can be seen in Figure 2.5.

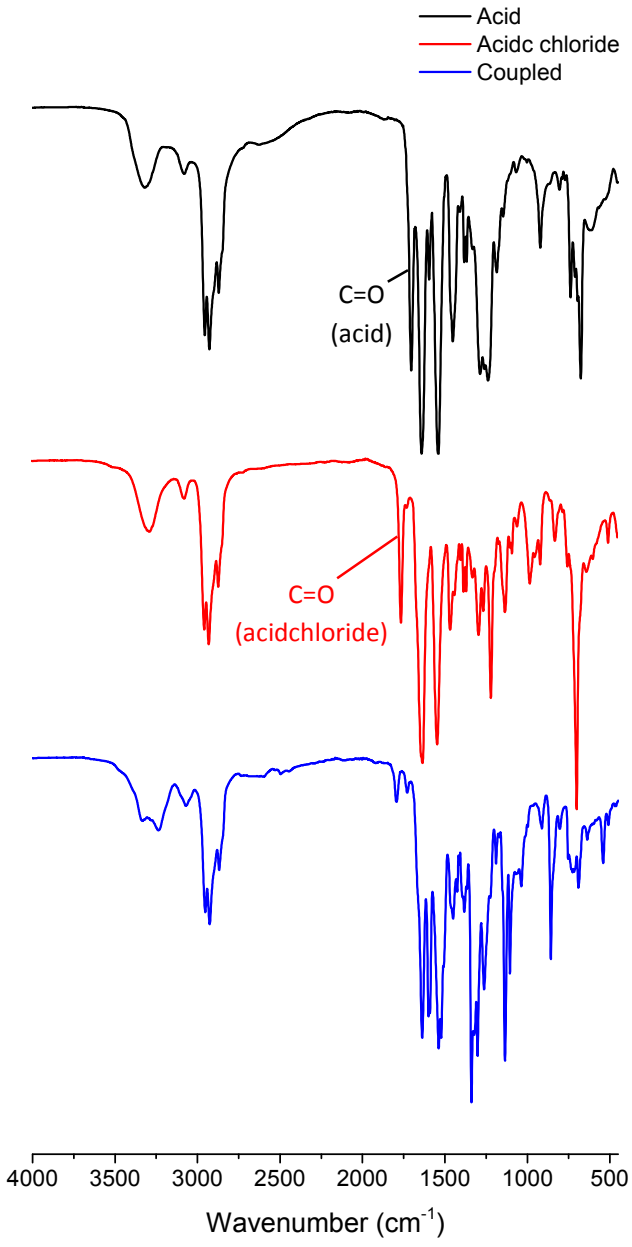

Figure 2.5: Infrared spectra of the reaction mixtures to check the conversion by the shift of the carbonyl peak.

The obtained product **9** was characterised using NMR, FT-IR and MALDI-TOF MS.

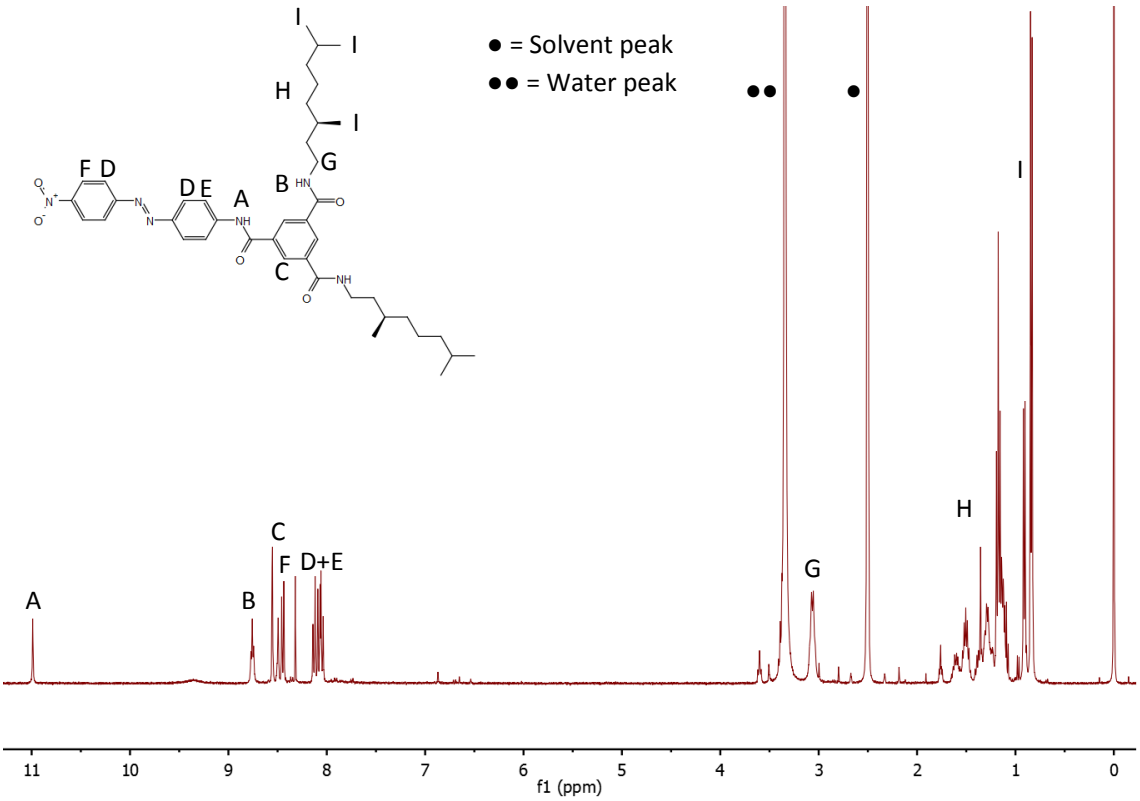

Figure 2.6: ^{1}H-NMR spectrum of compound **9** after purification.

All signals in the ^{1}H-NMR of compound **9** can be assigned as shown in Figure 2.6. Integrals and peak positions correspond with the expected values, showing successful coupling of the azo-compound to the BTA.

The IR spectrum of compound **9** shows the expected peaks belonging to the N-H, C-H, C=O and N-O stretches, see Figure 2.7. Furthermore, the peak at 1763 cm^{-1} belonging to the acid chloride, present in the reaction mixture (see Figure 2.5) is completely gone after purification.

With MALDI-ToF MS peaks were found corresponding to the hydrogen and sodium adduct of compound **9** (see Figure 2.8). From the NMR, IR and MALDI-ToF MS results, a successful synthesis of BTA **9**, in good purity, can be concluded.

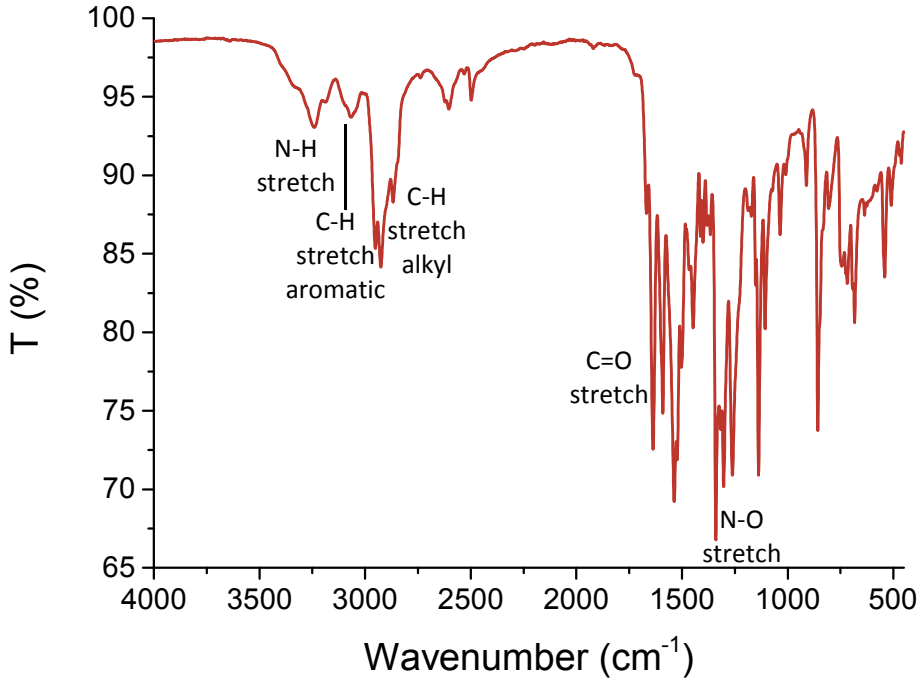

Figure 2.7: The IR spectrum of compound **9**.

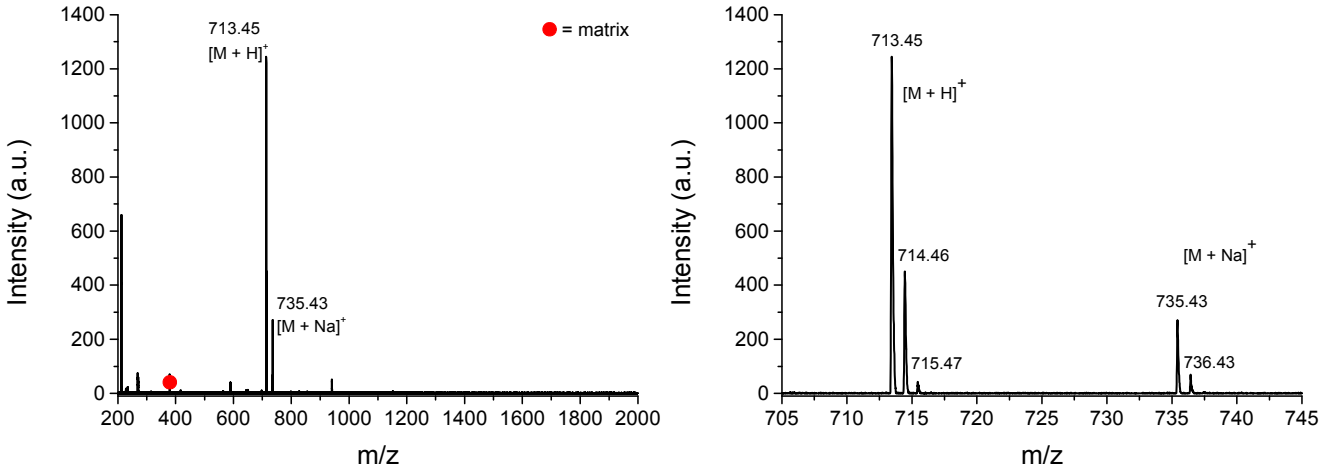

Figure 2.8: (Left) MALDI-ToF MS spectrum of compound **9**. (Right) zoom in of the spectrum showing the hydrogen and sodium adduct isotope peaks.

The nitro group of BTA **9** had to be converted into an amine while the azo-bond has to remain intact as already explained before. For this reason the Zinnin reduction was chosen for this task, since this reduction does not affect the azo-bond. BTA **9** was dissolved in DMSO to which water with sodiumsulphide nonahydrate was added. The reaction was stirred during 8 hours in a microwave reactor. The product was purified using an extraction in chloroform against water. Purification with column chromatography gave the product **2** in a 33% yield.

Column chromatography was used again for the purification of BTA **2**, assuming that the stability of the molecules amide bond was changed due to the conversion of the nitro group into an amine. However, also hydrolysis of the amide bond between the BTA-core and the azo-compound takes place on a silica column. Trituration with diethyl ether again proved to be a better purification method. Unfortunately also (almost) complete hydrolysis is observed during the work up of the reaction mixture on larger scale, when the DMSO-water mixture was removed *in vacuo*. Also in an alternative pathway, when water was added in order to do an extraction of the product with chloroform, hydrolysis was observed.

The obtained compound **2** was characterised using NMR, FT-IR and MALDI-TOF MS.

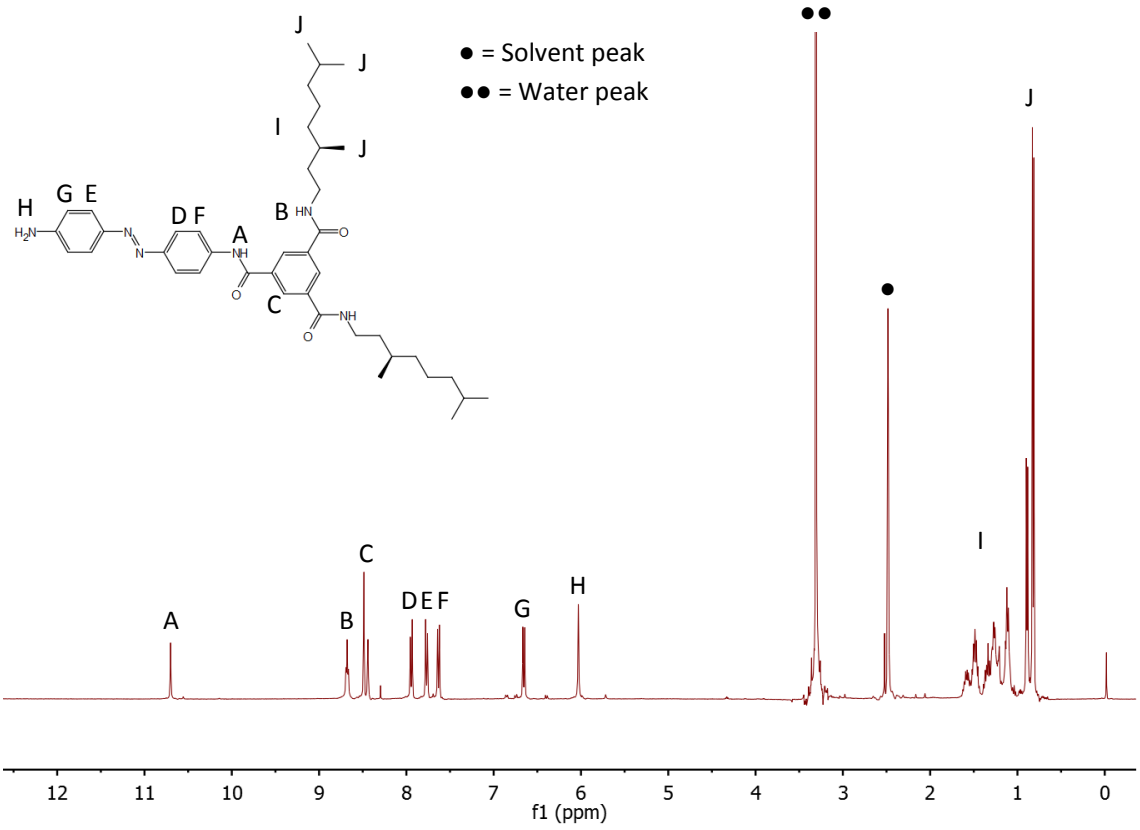

Figure 2.9: ^{1}H-NMR spectrum of compound **2**.

All signals in the ^{1}H-NMR of compound **2** are shifted to the right compared to the NMR of **9**, due to the exchange of the nitro group for the electron rich amine. All signals can be assigned to compound **2** as shown in Figure 2.9. The small peaks at 6.85, 6.74 and 6.39 ppm correspond to protons of the *cis* form of the molecule.

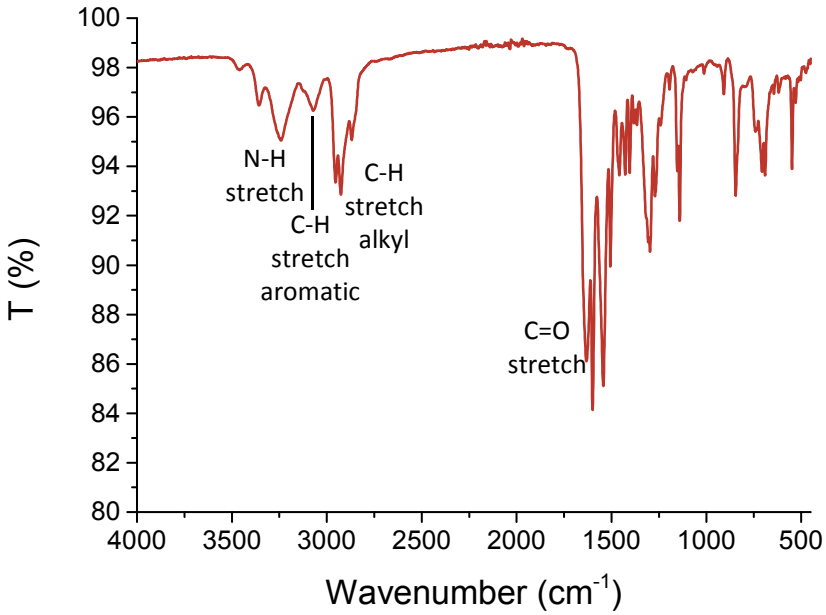

Figure 2.10: The IR spectrum of compound **2**.

The IR spectrum of compound **2** shows the disappearance of the peak belonging to the nitro group as expected and is similar to the spectrum of **9** (shown in Figure 2.7).

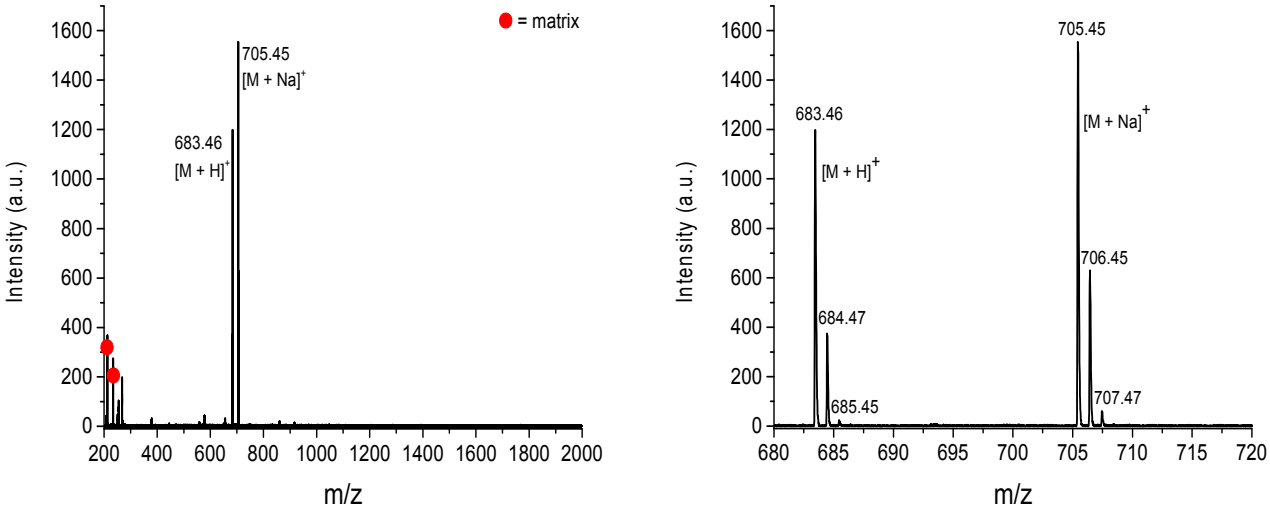

Figure 2.11: (Left) MALDI-ToF MS spectrum of compound **2**. (Right) zoom in of the spectrum showing the hydrogen and sodium adduct isotope peaks.

With MALDI-ToF MS mass peaks were found corresponding to the hydrogen and sodium adduct of BTA **2** (see Figure 2.11). A successful synthesis of BTA **2**, in good purity, can be concluded from the NMR, IR and MALDI-ToF MS results.

Coupling with succinic anhydride

To be able to graft BTA **2** on the surface of silica beads, it had to be coupled to succinic anhydride first. This was done on a small scale by dissolving **2** in THF and succinic anhydride in presence of triethylamine and 4-dimethylaminopyridine letting it react for 18 hours at reflux under argon atmosphere. After removing the solvent *in vacuo*, the crude was dissolved in ethyl acetate, extracted with a diluted ammonium chloride solution, and dried over magnesium sulphate. Due to the low amount of crude only the raw synthesis-product is analysed with NMR and MALDI-ToF MS. The presence of product **11** was verified making use of NMR and MALDI-ToF MS, showing successful coupling of **2** succinic anhydride. No purification of the product was done due to the low amount of material.

Alternative route avoiding hydrolysis

Since the amide bond is easily hydrolysed during the work up of the reduction step, which has to be done in an aqueous solution, this is not a practical synthesis route. Therefore, another synthesis route was examined (see Scheme 2.6), in which the azo-compound would be coupled to succinic anhydride first. Only after reducing the nitro group into an amine, the coupling between the azo-compound and the BTA core had to be done. In this way the reduction step, leading to hydrolysis of the amide bond between the azo-compound and the BTA core, is avoided after formation of this amide bond. In this way the molecule is also suitable for the coupling to beads immediately.

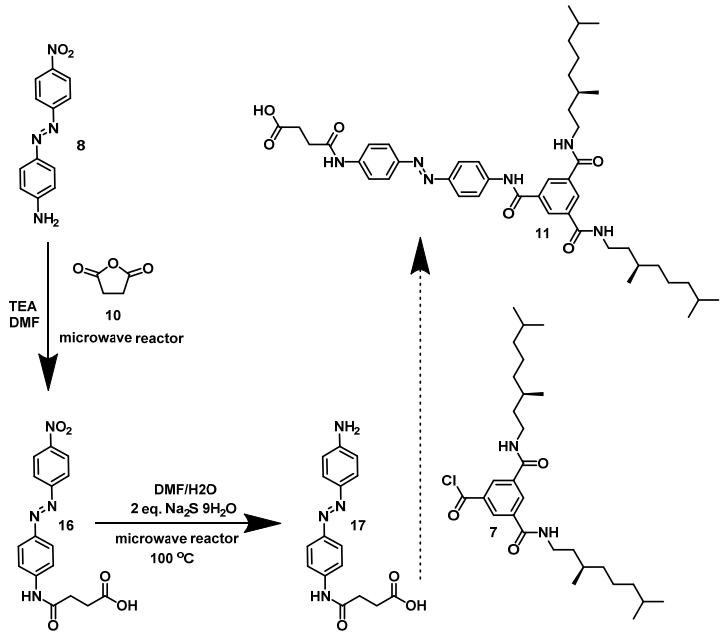

Scheme 2.6: Alternative synthetic route to obtain a BTA suitable for coupling directly.

In order to do the coupling, 4-(4-nitrophenylazo)aniline was dissolved in dimethylformamide (DMF) with a small amount of TEA and succinic anhydride was added. The reaction was done in a microwave reactor for 5 min at 75 °C, followed by 20 min at 140 °C. The reaction was stopped and trituration was done with chloroform resulting in a not completely pure material. Trituration with

diethyl ether did not work either and column chromatography was avoided since azo-compounds stick to the silica in large amounts. Since the amount of material was small, the next step was done with the material without further purification.

As the nitro group had to be reduced, the molecule was dissolved in DMF and after addition of an aqueous solution of sodium sulphide the mixture was placed in a microwave reactor for 8 hours at 100 °C. After the reaction, the solvents were removed *in vacuo.* The presence of the product was verified using MALDI-ToF MS and NMR, confirming the successful synthesis of **17**. No purification is done due to the small amount of material.

2.4 Conclusions

The light responsive BTAs **1** and **2** were designed and synthesized successfully. The first approach to synthesize BTA **2** showed that a BOC-protection is possible, but the purification of the product from the statistical mixture proved to be unsuccessful. Making use of an asymmetric azo-compound as starting material, BTA **2** could be synthesized on small scale. Unfortunately, upscaling of this procedure gives problems with the work-up of the reaction mixture. The observed hydrolysis during this work up might be due to the presence of a large amount of water during the work-up in combination with the weak amide bond between the BTA core and the azo-compound. Therefore a new synthesis route was designed in which a combination of water with the presence of the weak amide bond is avoided. The synthesis route was not completely evaluated but might provide solution for the problem. This should be evaluated in further research. The coupling of BTA **2** with succinic anhydride is tested and gave molecule **11**. When this reaction could be performed on a larger scale it is possible to couple the light responsive BTA **11** to the silica beads in the following step.

2.5 Experimental section

Materials

Chemicals and solvents were purchased from Sigma-Aldrich, Acros Organics, or TCI Europe and used as received, unless specified otherwise. All solvents were purchased from Biosolve. Chloroform and THF were dried over 4 Å molecular sieves before use. Compound **5** was kindly provided by Jolanda Spiering. Triethylamine was dried and stored over KOH pellets. Deuterated compounds were obtained from Cambridge Isotopes Laboratories and stored over 4 Å molecular sieves. All reactions were carried out under argon atmosphere unless stated otherwise. Reactions were followed by thin-layer chromatography (TLC) using 60-F254 silica gel plates from Merck and visualized by UV light at 254 nm and/or ninhydrin- or vanillin- staining. Flash column chromatography was performed on a Biotage Isolera II Chromatography system using SNAP columns.

Instrumentation

All ^{1}H-NMR and ^{13}C-NMR spectra were recorded on a Varian Mercury Vx 400 MHz and/or a Varian 400 MHz (400 MHz for ^{1}H-NMR and 100 MHz for ^{13}C-NMR). Proton chemical shifts are reported in ppm (δ) downfield from trimethylsilane (TMS) using the resonance frequency of the deuterated solvent as the internal standard. Peak multiplicity is abbreviated as s: singlet; d: doublet; t: triplet; m: multiplet; dd: doublet of doublets; td triplet of doublets. Carbon chemical shifts are reported in ppm (δ) downfield from TMS using the resonance frequency of the deuterated solvent as the internal standard. Matrix assisted laser absorption/ionization mass spectra were obtained on a PerSeptive Biosystems Voyager DE-PRO spectrometer using α-cyano-4-hydroxycinnamic acid (CHCA) or trans-2-[3-(4-tert-butylphenyl)-2-methyl-2-propenylidene]malononitrile (DCBT) as matrix. Infrared spectra were recorded using a Perkin Elmer Spectrum Two FT-IR spectrometer equipped with a Perkin Elmer Universal ATR Two Accessory. Freeze drying was achieved using a Salmenkipp Christ Alpha 2-4 LD Plus freeze dry system equipped with a Vacuubrand RC6 Chemistry Hybrid vacuum pump. The microwave reactor used was a Biotage Initiator plus instrument.

Synthetic procedures

Tris(4-(*E*)-phenyldiazenyl)phenyl)-benzene-1,3,5 tricarboxamide 1

4-Phenylazoaniline (**4**) (372.0 mg, 1.89 mmol) was dissolved in dry THF (2.5 mL) and triethylamine (0.5 mL, 3.58 mmol) was added. A solution of 1,3,5-benzenetricarbonyl trichloride (**3**) (99.7 mg, 0.43 mmol) in dry THF (5 mL) was added dropwise to the solution of **4**. The resulting mixture was stirred at room temperature for 48 h under argon atmosphere and filtered. The filtrate was concentrated *in vacuo* and precipitated in MeOH. The solid precipitates were collected and dried to give BTA **1** (134.3 mg, 0.18 mmol, 42%) as an orange powder.

^{1}H-NMR (400 MHz, DMSO): δ (ppm): 10.97 (s, 3H, C-(C=O)-NH-C),8.82 (s, 3H, (C=O)-C-CH-C-(C=O)), 8.12 (d, *J* = 9.2 Hz, 6H, CH-CH=C-N=N), 8.00 (d, *J* = 9.2 Hz, 6H N=N-C=CH-CH=CH), 7.90 (d, *J* = 7.6 Hz 6H, NH-CH-CH=C-N=N), 7.59 (m, 9H, N=N-C=CH-CH=CH)

^{13}C-NMR (100 MHz, DMSO): δ (ppm): 165.22 (C=O); 152.49, 148.49, 142.48, 135.74, 129.91, 124.06, 122.84, 121.05, 109.99 (aromatic carbons).

FT-IR (ATR) ν (cm^{-1}): 844, 1153,1250, 1302, 1321, 1404, 1500, 1531, 1596, 1668, 3069, 3319.

MALDI-TOF-MS: calculated for $C_{45}H_{33}N_9O_9$ Mw = 747.27 g/mol, observed m/z = 748.28 [M+H]+, 770.26 [M+Na]+.

***N*,*N*-Bis((R)-3,7-dimethyl-octylaminocarbonyl-*N*-phenylbenzene-1,3,5 tricarboxamide 18**

3,5-Bis(R)-3,7-dimethyl-octylaminocarbonyl) benzoic acid chloride (**7**) (24 mg, 0.047 mmol) was dissolved in 2 mL dry chloroform and placed in an ice bath. To this solution a solution of aniline (5 mg, 0.023 mmol) and TEA (27 µL, 0.19 mmol) in 2 mL dry chloroform was added drop wise. After 18 h the reaction was stopped after checking the conversion with IR. The solvents were removed *in vacuo*, and the resulting mixture was dissolved in 10 mL chloroform. The mixture was extracted with 1 M HCl 5 mL twice and twice with a saturated NaCl solution 5 mL. After drying over $MgSO_4$ the solvent was removed *in vacuo* giving the product (23 mg, 0.041 mmol, 87%).

4,4'-Azodianiline 12

4-(4-Nitrophenylazo)aniline (25.1 mg, 0.10 mmol) was dissolved in 6 mL 1,4-dioxane. A solution of sodiumsulphide nonahydrate (49.7 mg, 0.21 mmol) in water (3 mL) was added. The reaction mixture was placed in a microwave reactor for 10 hours at 100 °C, the solvents were removed *in vacuo*. After

dissolving the mixture in chloroform (20 mL) an extraction with water (20 mL) was done twice. The resulting solution was dried over $MgSO_4$ and the solvent removed *in vacuo* yielding the product (15 mg, 0.071 mmol, 71%) as an orange powder.

3,5-Bis(R)-3,7-dimethyl-octylaminocarbonyl) benzoic acid chloride 7

3,5-Bis(R)-3,7-dimethyl-octylaminocarbonyl) benzoic acid (**5**) (999.8 mg, 2.04 mmol) and 1-chloro-*N,N,*-2-trimethyl-1-propenylamine (**6**) (314.4 mg, 2.35 mmol) were dissolved in dry chloroform (80 mL). The mixture was stirred for 2 h at room temperature under argon atmosphere, while the conversion was followed by IR by following the carbonyl peak at 1704 cm^{-1}. The mixture was concentrated *in vacuo* and the residue was dried thoroughly using high vacuum to assure the removal of the excess of 1-chloro-*N,N,*-2-trimethyl-1-propenylamine. The resulting product **7** was directly used for further synthesis.

***N*,*N*-Bis(*R*)-3,7-dimethyloctyl)-*N*-(4-((*E*-(4-nitrophenyl)diazenyl)phenyl)benzene-1,3,5-tricarboxamide 9**

3,5-Bis(*R*)-3,7-dimethyl-octylaminocarbonyl) benzoic acid chloride (**7**) (1.01 g, 1.99 mmol) and triethylamine (1.17 mL, 15.83 mmol) were dissolved in dry THF (80 mL) and cooled with an ice bath, to 0 °C. A solution of 4-(4-nitrophenylazo)aniline (**8**) (501.2 mg, 2.06 mmol) in dry THF (80 mL) was added dropwise to the solution of **7**. The mixture was allowed to warm up to room temperature and was stirred for 24 hours. THF and triethylamine were removed *in vacuo* and the product was purified using trituration with diethyl ether (2 times, 60 mL). The product **9** was obtained as an orange coloured solid (979.7 mg, 1.37 mmol, 69 %).

^{1}H-NMR (200 MHz, DMSO): δ (ppm): 10.95 (s, 1H, C-(C=O)-NH-C), 8.71 (t, *J* = 5.2 Hz, 2H, C-(C=O)-NH-CH_2), 8.55 (s, 2H, (C=O)-C-CH-C-(C=O)), 8.49 (s, 1H, (C=O)-C-CH-C-(C=O)), 8.44 (d, *J* = 1.4 Hz, 2H, O_2N-C=CH-CH=C), 8.07 (td, *J* = 2 hz, 6H, CH-CH=C-N=N-C=CH-CH=C-NH), 1.78–1.02(m, 24H, NH-CH_2-CH_2-CH(-CH_3)-CH_2- CH_2-CH_2(-CH_3)$_2$, 0.94–0.76 (dd, *J* = 6.2 Hz, *J* = 6.6 Hz, 18H, CH_2-CH(-CH_3)-CH_2- CH_2-CH_2(-CH_3)$_2$)

^{13}C-NMR (100 MHz, THF): δ (ppm): 164.71 (C=O); 155.59, 148.27, 143.48, 135.59, 135.06, 128.47, 128.10, 124.28, 128.03, 122.82, 119.75 (aromatic carbons); 39.05, 37.56, 36.98, 36.57, 30.45, 27.70, 21.74, 18.72 (aliphatic carbons).

FT-IR (ATR) υ (cm^{-1}): 859, 1106, 1135, 1271, 1297, 1302, 1339, 1522, 1601, 1641, 1793, 2869, 2926, 2954,3073, 3335.

MALDI-TOF-MS: calculated for $C_{41}H_{56}N_6O_5$ Mw = 712.43 g/mol, observed m/z = 713.45 [M+H]+, 735.43 [M+Na]+.

***N*-(4-((*E*)-(4-Aminophenyl)diazenyl)phenyl)-*N*,*N*-bis(R)-3,7-Dimethyloctyl)-benzene-1,3,5-tricarboxamide 2**

To BTA **9** (99.9 mg, 0.14 mmol), which was dissolved in DMSO (12 mL), a solution of sodiumsulphide nonahydrate (50.4 mg, 0.21 mmol) in water (2 mL) was added. This was placed in a microwave reactor for 8 hours at 100 °C. The solvents were removed *in vacuo* and the reaction product was dissolved in chloroform and extracted with water. The product was purified using column chromatography (going from pure chloroform to a mixture of 20% ethyl acetate-chloroform). An orange solid was obtained as product **2** (33 mg, 0.05 mmol, 34%).

As an alternative work-up, trituration with diethyl ether (5 mL) was done resulting in a higher yield (52%). The product was freeze dried before characterization was performed.

^{1}H-NMR (400 MHz, DMSO): δ (ppm): 10.70 (s, 1H, C-(C=O)-NH-C), 8.68 (t, *J* = 5.6 Hz, 2H, C-(C=O)-NH-

CH_2), 8.49(s, 2H, (C=O)-C-C<u>H</u>-C-(C=O)), 8.44 (s, 1H, (C=O)-C-C<u>H</u>-C-(C=O)) 7.94 (d, *J* = 8.8 Hz, 2H, C=C<u>H</u>-CH=C-NH), 7.77 (d, *J* = 8.8 Hz, 2H, H_2N-C=CH-C<u>H</u>-C), 7.63 (d, *J* = 8.8 Hz, 2H, C=CH-C<u>H</u>=C-NH), 6.66 (d, *J* = 8.8 Hz, 2H, H_2N-C=C<u>H</u>-CH=C), 6.03 (s, 2H, CH=C-N<u>H_2</u>), 1.64–1.00(m, 24H, NH-CH_2-C<u>H_2</u>-C<u>H</u>(-CH_3)-C<u>H_2</u>-C<u>H_2</u>-C<u>H_2</u>(-CH_3)$_2$, 0.94–0.76 (dd, *J* = 6.8 Hz, *J* = 6.4 Hz, 18H, CH_2-CH(-C<u>H_3</u>)-CH_2- CH_2-CH_2(-C<u>H_3</u>)$_2$)

^{13}C-NMR (100 MHz, DMSO): δ (ppm): 165.56, 165.40 (C=O); 152.96, 148.91, 143.29, 140.72, 135.54, 129.28, 125.33, 122.76, 121.02, 113.83 (aromatic carbons); 37.90, 37.05, 36.51, 30.42, 27.83, 24.43, 22.91, 19.93 (aliphatic carbons).

FT-IR (ATR) υ (cm^{-1}): 846, 1141, 1271, 1297, 1506, 1543, 1600, 1632, 2868, 2926, 2954, 3072, 3241, 3358.

MALDI-TOF-MS: calculated for $C_{41}H_{56}N_6O_3$ Mw = 682.46 g/mol, observed m/z = 683.46 [M+H]+, 705.44 [M+Na]+.

(*E*)-4-((4-((4-Nitrophenyl)diazenyl)phenyl)amino)-4-oxobutanoic acid 16

4-(4-Nitrophenylazo)aniline **8** (49.8 mg, 0.21 mmol), succinic anhydride **10** (26.1 mg, 0.26 mmol) and TEA (100 µL, 0.70 mmol) were dissolved in 5 mL DMF. The mixture was placed in a microwave reactor 5 minutes at 75 °C and 20 minutes at 140 °C. The solvents were removed *in vacuo* and a trituration was performed using 5 mL chloroform and 5 mL diethyl ether. The resulting mixture **16** (28.02 mg) was used without further purification.

(*E*)-4-((4-((4-Aminophenyl)diazenyl)phenyl)amino)-4-oxobutanoic acid 17

(*E*)-4-((4-((4-Nitrophenyl)diazenyl)phenyl)amino)-4-oxobutanoic acid **16** (28.02 mg, 0.082 mmol) was dissolved in 3 mL DMF, to which a solution of sodiumsulphide nonahydrate (39.29 mg, 0.163 mmol) in 2 mL water was added. After 8 h in the microwave reactor (100 °C) the reaction was stopped, the solvents were removed *in vacuo*, and conversion to **17** was checked with TLC, NMR and MALDI-ToF MS. No purification was performed due to the small amount of material.

2.6 References

1. S. Lee, S. Oh, J. Lee, Y. Malpani, Y.-S. Jung, B. Kang, J. Y. Lee, K. Ozasa, T. Isoshima, S. Y. Lee, M. Hara, D. Hashizume and J.-M. Kim, *Langmuir*, 2013, **29**, 5869-5877.
2. J. Roosma, T. Mes, P. Leclère, A. R. A. Palmans and E. W. Meijer, *J. Am. Chem. Soc.*, 2008, **130**, 1120-1121.
3. N. Zinnin, *J. Prakt. Chem.*, 1842, **1**, 149.

Chapter 3: Investigating the effect of the *trans-cis* isomerization on the self-assembly behaviour of azo-containing BTAs

3.1 Introduction

Combining an azo-functionality with BTA motifs gives rise to interesting behaviour as shown by Lee *et al.*[1] The conformational change of the azo bond upon isomerization is used in their research to disrupt the self-assembly of the BTAs. In Figure 3.1 the absorption spectra of the symmetric light responsive BTA are shown upon irradiation with UV light and subsequently with visible light. Irradiation with UV light leads to a decrease of the peak at 365 nm belonging to the *trans* state of the molecule, simultaneously an increase of the peak at 440 nm, belonging to the *cis* state, is observed. This is reversed when the sample is irradiated with visible light.

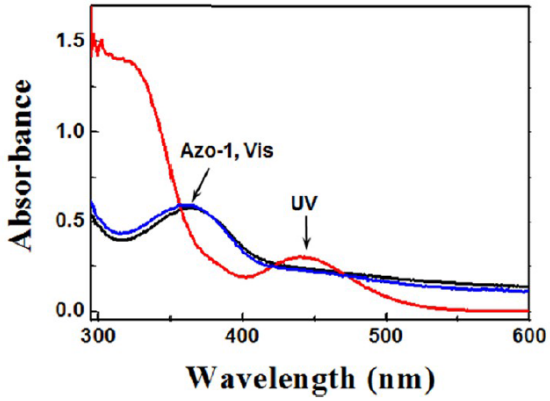

Figure 3.1: UV-Vis spectra of BTA **1** (10 mM) in 50% DMSO-H_2O before (black) and after (red) irradiation (UV 330-385 nm) for 30 sec. And after irradiation (blue) with visible light for 2 min (460-490 nm).[1]

The isomerization of an azo-bond is already used in liquid crystals and can be used to switch between the cholesteric and nematic phase.[2] Furthermore, the pitch of liquid crystals can be influenced when an azo-bond is incorporated.[3] Katayama *et al.* investigated the isomerization of the azo bond of a liquid crystalline material irradiating the film with UV light.[4] They observed that a change of ordering takes place upon irradiation, and that this change in the ordering travels a few microns into the material layer.

The conformational change can also be used in order to produce micro-actuators as shown by van Oosten *et al.*[5] By introducing a gradual orientation change of the liquid crystals through the film an upward bending splayed actuator was created. In their research they created modular artificial cilia making use of the properties of the azo bond upon isomerization (see Figure 3.2).

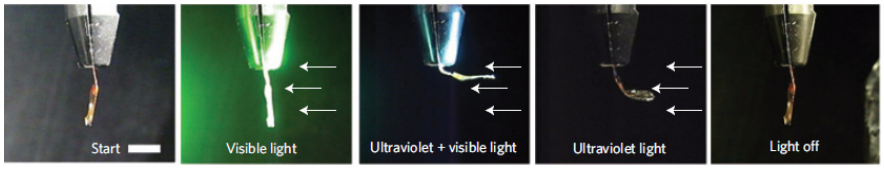

Figure 3.2: Liquid-crystal network actuator influenced by irradiation with light.

In this chapter we study the isomerization behaviour of light-responsive BTAs and the effect of this isomerization on the assembly behaviour, due to the conformation change that accompanies the isomerization. Making use of an asymmetric BTA it is possible to change the number of azo-functionalities in the BTA and to improve the solubility of the BTA making use of less bulky side chains.

To investigate the isomerization behaviour of the light responsive BTAs, first the *cis-trans* behaviour of symmetric BTA **1** was investigated followed by that of asymmetric BTA **2** (see Figure 3.3).

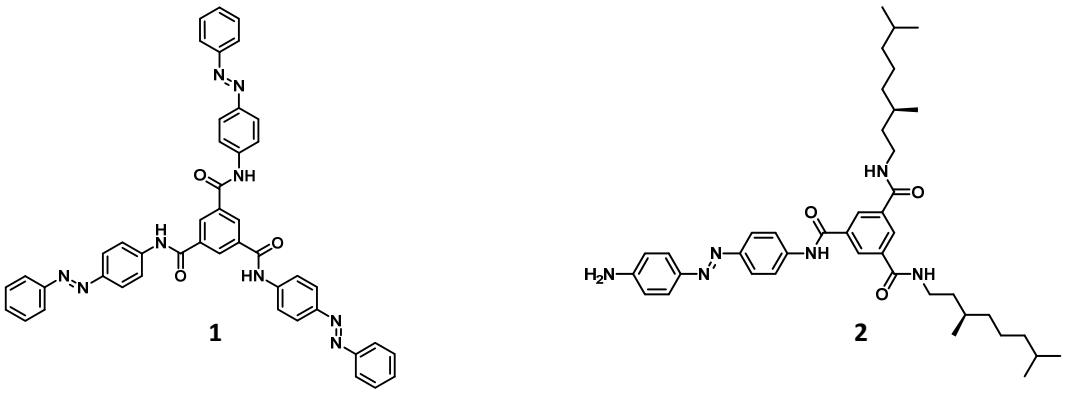

Figure 3.3: Schematic representation of the symmetric light responsive BTA **1** (left), and the asymmetric variant **2** enabled for coupling (right).

3.2 Characterization of 1 and 2 in bulk

The BTAs were characterized in bulk, making use of differential scanning calorimetry (DSC), polarized optical microscopy (POM) and for BTA **2** also infrared (IR) spectroscopy and wide angle X-ray scatting (WAXS) was used. Using POM no transitions or birefringence were observed for compound **1** up to 300°C. With DSC the melting point of the compound was not observed up to 250 °C, only a very small glass like transition at 108 °C was observed.

Using DSC the temperature-dependent transitions of BTA **2** were investigated. A melting temperature of 188 °C of the material was determined during the second heating run. To investigate this transition to greater extent it was investigated using POM.

Using POM the solid state packing of the material was examined upon temperature change (see Figure 3.4). The material showed to be birefringent, and the birefringence disappeared upon heating the sample to around 205 °C (see Figure 3.4 a-c), slightly higher than observed with DSC due to the

poor temperature control. The loss of birefringence around 200 °C was also observed in previous studies for other BTAs, showing that our findings are in accordance with those results.[6] When the sample was cooled down, to 200 °C, the birefringence reappeared, and the material seemed to be more ordered than before (see Figure 3.4 d-h). When some pressure was applied on the sample, flowing of the material was still observed indicating that the material has liquid crystalline properties (see Figure 3.4 i).

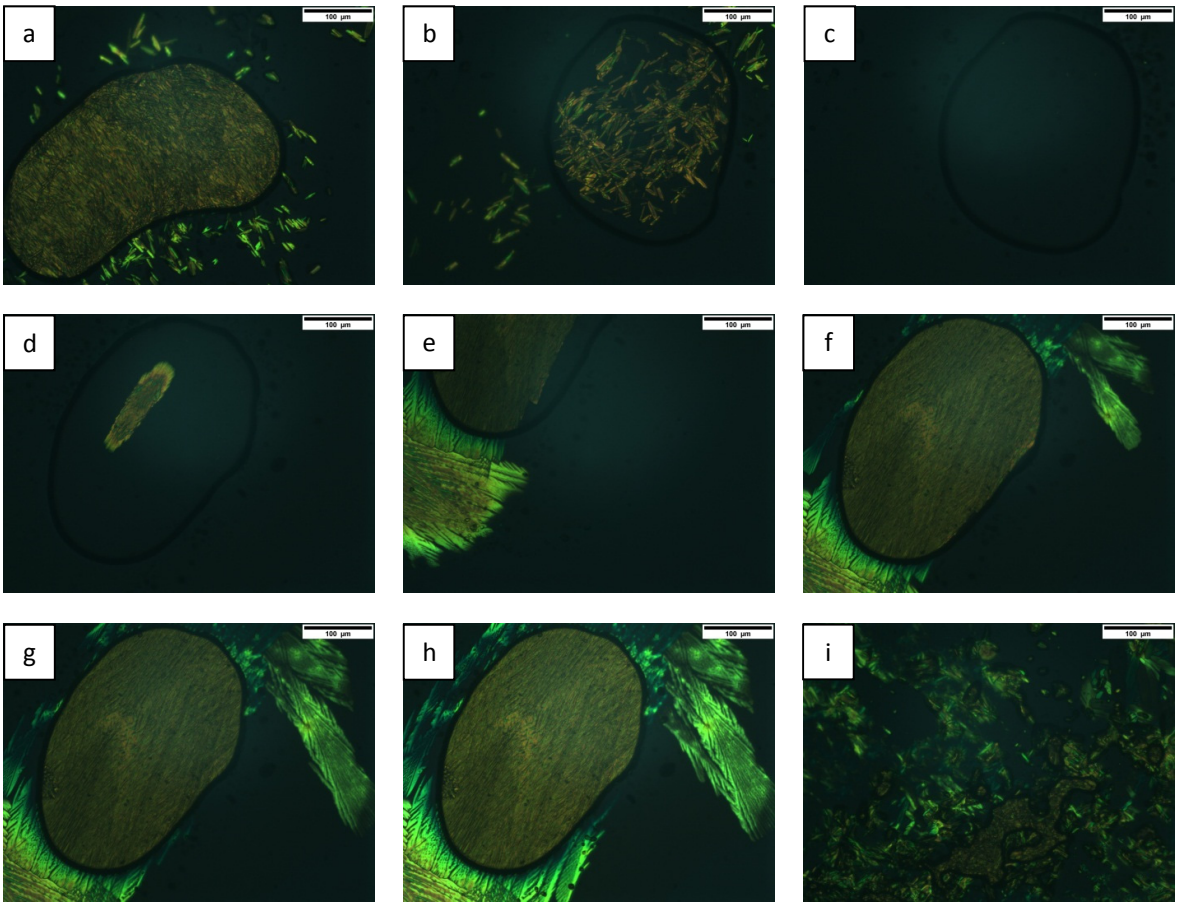

Figure 3.4: POM images of BTA **2** upon heating a-c and cooling d-i of the sample, picture i was taken after applying pressure on the sample and flow was observed.

To investigate the solid state of the material in more detail and to investigate if the material is indeed a liquid crystal WAXS was used.

WAXS was used in order to examine the packing of BTA **2** at variable temperatures. When the temperature was increased above 60 °C more peaks were observed in the WAXS spectra of the BTA, these peaks disappear again at temperatures above 190 °C (see Figure 3.5). The appearance of these peaks indicates crystallinity in this temperature regime, and these peaks were used to investigate the packing of the material. In the WAXS data the reflections at $\sqrt{3}$, $\sqrt{4}$, $\sqrt{7}$, $\sqrt{9}$, $\sqrt{12}$, $\sqrt{13}$ and $\sqrt{19}$ were observed indicating hexagonally packed cylinders. This packing is also found for other BTAs in previous studies, and was therefore also expected.[7] However, the intensity usually decreases going from $\sqrt{3}$ to $\sqrt{4}$, this is not the case in our measurements, possibly due to the presence of another packing in the material. The peak at 1.77 $Å^{-1}$ corresponds to a distance of 3.54 Å and this is known to

be the interdiscotic distance for BTAs. This peak, corresponding to the interdiscotic distance, completely disappeared at 197 °C as expected based on POM and DSC, as the crystal melts. Furthermore, the principal peak q^* at 0.35 $Å^{-1}$ corresponds to a distance of 20.7 Å for parameters a and b in its crystal lattice, representing the distance between the columns (see Figure 3.6). As the temperature was decreased, not all peaks reappear as clearly as expected when the crystallinity comes back, this might be due to too fast cooling of the sample. The reappearance of the principal peak shows the reformation of the columns. To confirm that the sample did not degrade during the measurement, NMR was measured of the sample after the heating. From this NMR it was concluded that BTA **2** remained unchanged by the WAXS measurement conditions.

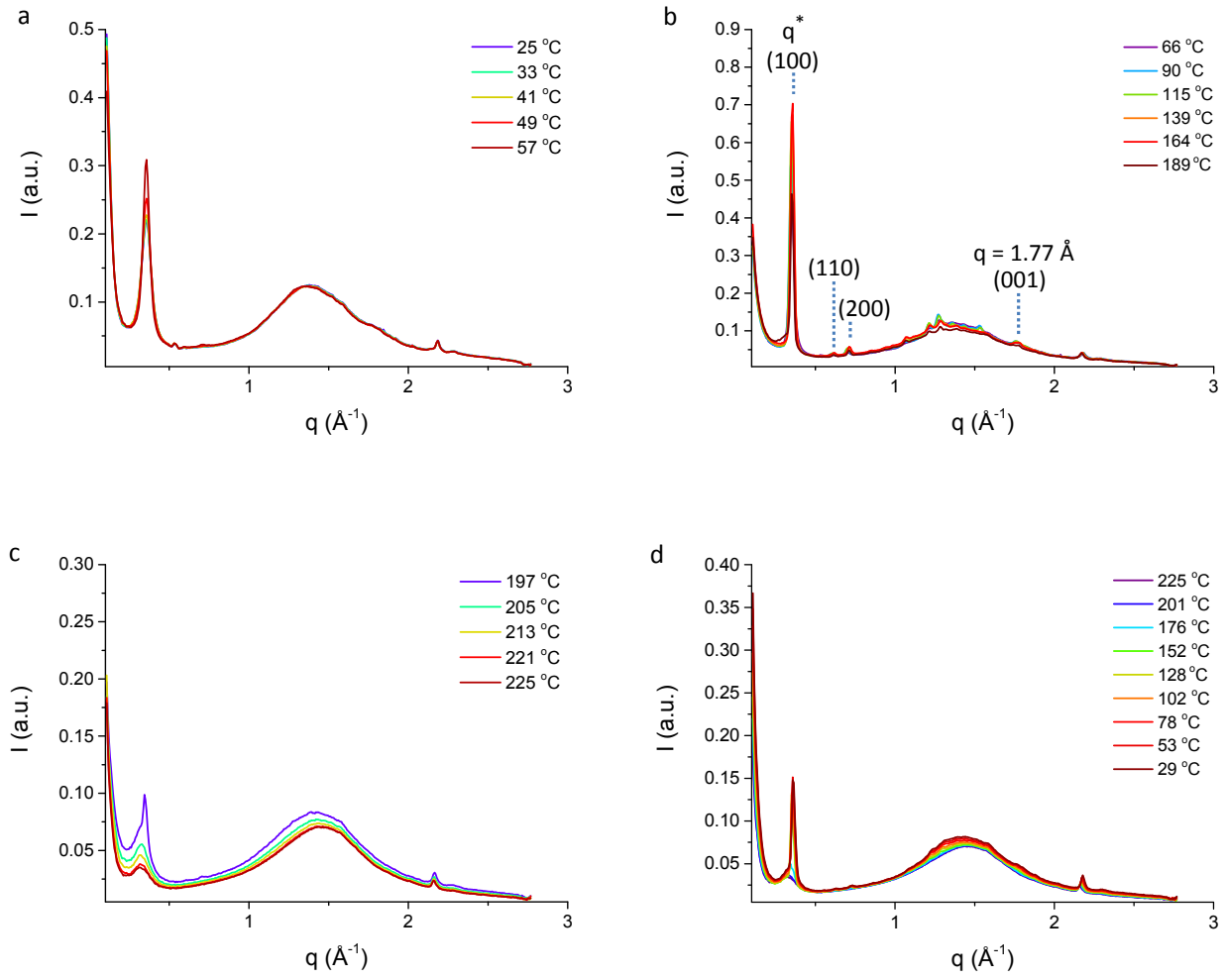

Figure 3.5: WAXS measurements of BTA **2** in solid state at a temperature range of 25 to 225 °C during heating (a-c) and cooling (d) of the sample.

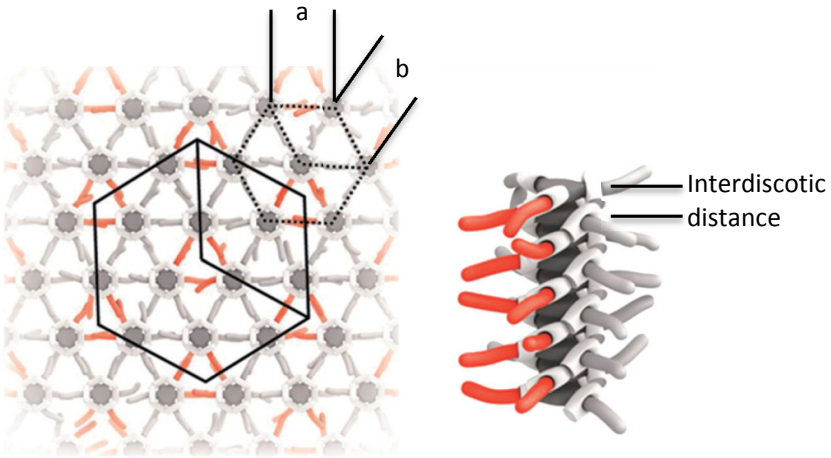

Figure 3.6: Schematic model for a hexagonal columnar packing.[7]

In comparison, the WAXS data of another BTA, see Figure 3.7, from B. Bögels are shown below in Figure 3.8. This BTA is known to be liquid crystalline at low temperature.

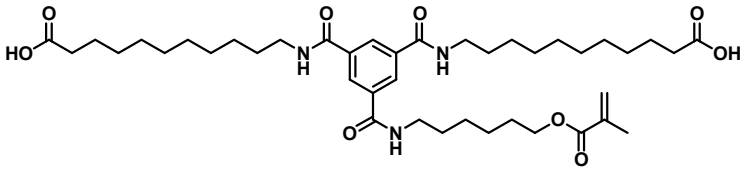

Figure 3.7: Structure of the BTA used as reference for the WAXS data.

The WAXS data of this BTA is depicted in Figure 3.8 at 20 and 35 °C. This molecule is known to be in its liquid crystalline state at 20 °C and in the liquid phase at 35 °C. As can be seen from Figure 3.8 the peaks corresponding to (110) (200) and (001) disappear when the molecule is heated and in its molten phase. The (001) peak corresponds to the interdiscotic distance of this BTA, and is also around 3.5 Å, since this distance does not vary much for different BTAs. In this case the intensity of the (100), (110) and (200) peaks decreases going from left to right in the figure, as is expected in WAXS data. The reason why this is not observed for BTA **2** is not known.

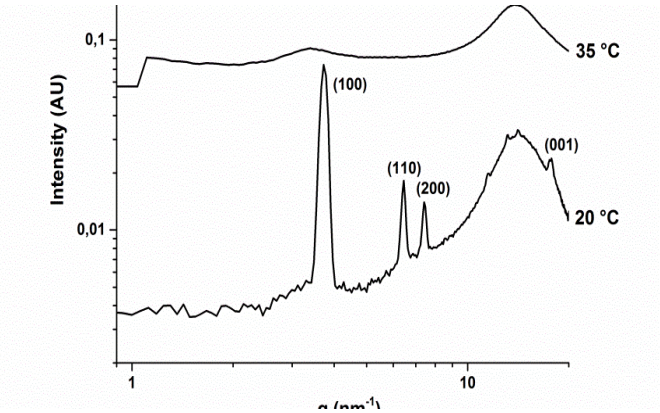

Figure 3.8: WAXS measurements of a liquid crystalline BTA.

Using WAXS the packing of materials can be examined, furthermore, IR spectroscopy can be used to investigate whether hydrogen bonds are present between molecules. Making use of IR spectroscopy the presence of hydrogen bonds, for BTA **2**, was examined in the solid state. This was done by checking whether the characteristic intermolecular hydrogen bonding peak is present in the IR spectrum. In solid state all peaks are generally less pronounced, compared to IR spectroscopy in solution. However, the characteristic H-bonding peak at 3240 cm^{-1} is still visible and strong, in comparison with the peak at 3360 cm^{-1}, in the IR spectrum of **2** (see Figure 3.9). In order to verify the hydrogen bonding in solid state, temperature-dependent IR-measurements were done.

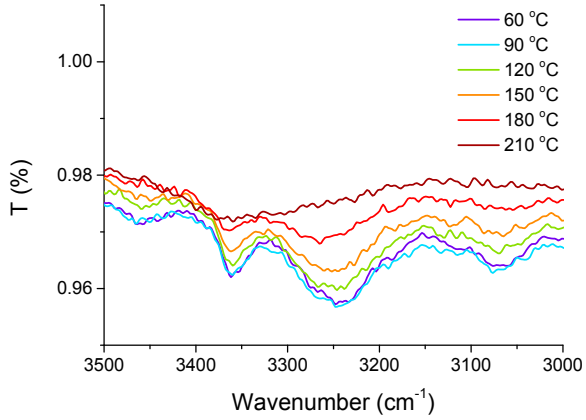

Figure 3.9: IR spectra of BTA **2** at different temperatures in solid state.

The temperature-dependent IR spectra show that the characteristic H-bonding peak is present in the IR spectrum of the BTA (from 60 to 150 °C). When the sample is heated above 180 °C it starts to decrease and shift to higher wavenumbers, indicating disruption of the H-bonds. At 210 °C the H-bonding peak is completely lost (see Figure 3.9). So the H-bonding is lost upon increasing the temperature, as was observed before.[8]

3.3 Investigating the isomerization of the symmetric azo-BTA

Next, the *trans-cis* isomerization of BTA **1** in solution was investigated, to get more information about the switching behaviour at lower concentrations, compared to the high concentrations (10 mM) Lee *et al.* applied.[1] UV-Vis spectra of BTA **1** (17.5 µM) were recorded before and after irradiating the samples with UV light and sometimes subsequently with visible light. Furthermore, to investigate whether self-assembly has an effect on the switching these measurements were done in two solvents, THF and 50% DMSO-H_2O. In THF, the molecule is molecularly dissolved according to Lee *et al*, while in 50% DMSO-H_2O aggregation is observed by Lee *et al.*

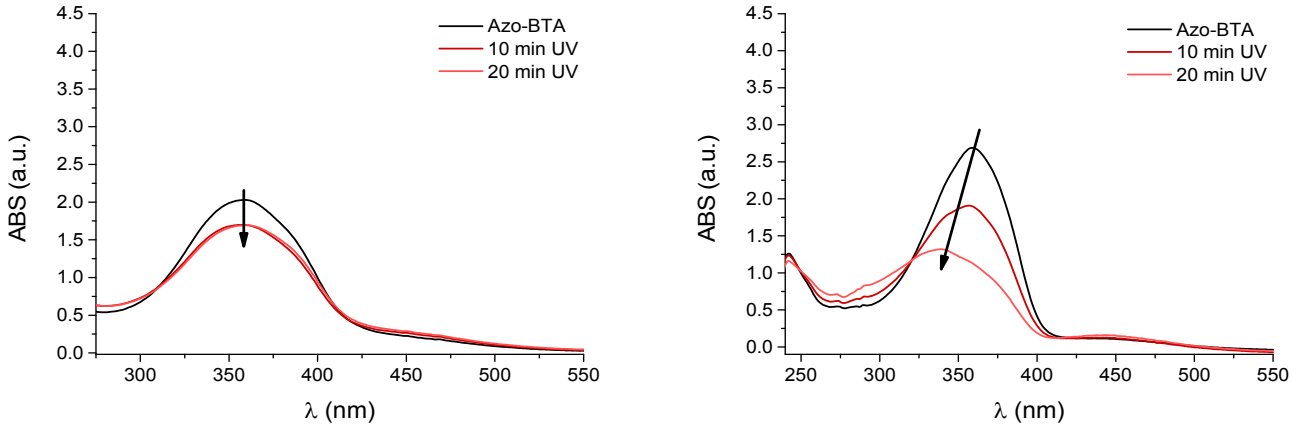

Figure 3.10: UV-Vis spectra of BTA **1** (17.5 µM), in 50% DMSO-H_2O (left) and THF (right), before (black) and after irradiation (red) with UV-light (350 nm) for 10 and 20 min, respectively.

Irradiating the molecule, in both DMSO-H_2O and THF with UV light (wavelength: 350 nm), leads to a decrease of the peak corresponding to the *trans* state of the molecule (see Figure 3.10). Moreover, λ_{max} in THF shifts from 358 nm to 342 nm and in the DMSO-H_2O mixture λ_{max} hardly shifts. In addition a small increase of the peak belonging to the *cis* state is observed (λ_{max} = 450 nm). These observations are similar to those Lee *et al.* have reported. However, the clear increase of the *cis* peak as reported is not seen in these measurements. In THF, additional to the decrease of the *trans* peak also a slight blue shift is seen, possibly due to conformational changes as a result of the isomerization. In order to go back from the *cis* to *trans* state the molecule, dissolved in THF, was irradiated with visible light (450 nm, see Figure 3.11).

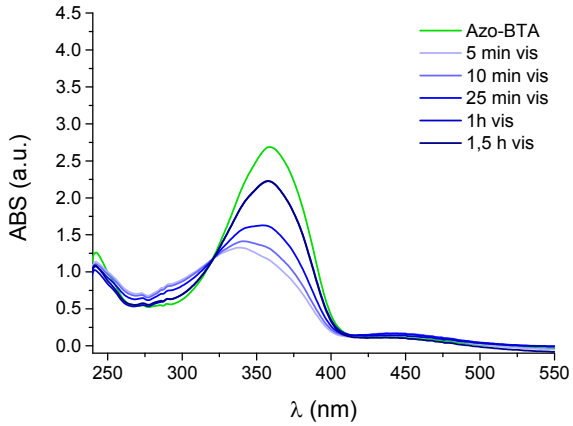

Figure 3.11: UV-Vis spectra of BTA **1** (17.5 µM) in THF before irradiation (black) and after irradiation (blue) with visible-light (450 nm) after different exposure times.

From irradiation of BTA **1** with visible light, it can be concluded that switching back to the *trans* conformation is possible. It takes more time to switch back to the *trans* state, compared to the switching from *trans* to *cis*, this observation is corresponding with the previous research.[1] Due to the shift of the λ_{max} of these spectra it was not possible to investigate the kinetics of the isomerization in an intensity versus time plot.

To verify whether the BTAs form aggregates or are molecularly dissolved, dynamic light scattering (DLS) experiments were performed in DMSO-H_2O mixtures and THF.

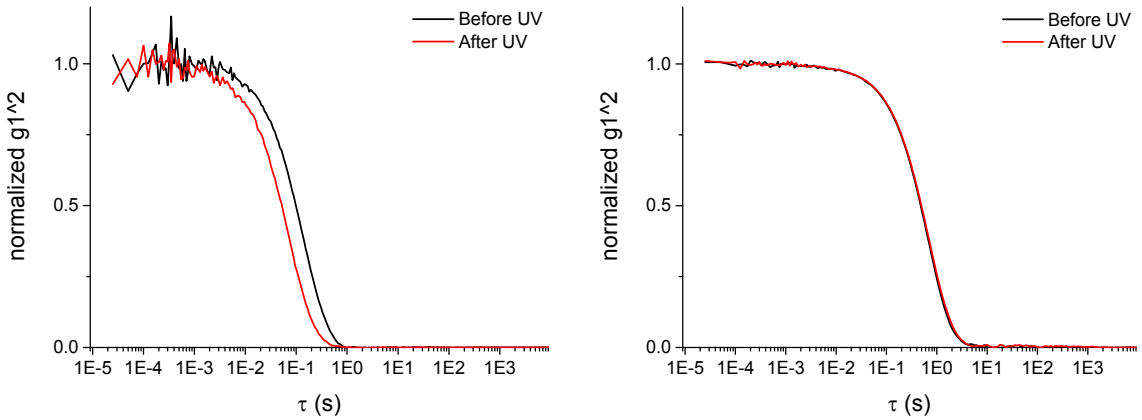

Figure 3.12: DLS curves of BTA **1** (17.5 µM) before (black) and after (red) irradiation with UV light. Left: 1% DMSO-H_2O. Right: 50% DMSO-H_2O

The results of the DLS measurements showed a longer correlation time in 50% DMSO-H_2O compared to a 1% DMSO-H_2O mixture, indicating that slightly larger aggregates are formed in the 50% DMSO-H_2O mixture (see Figure 3.12). This is not as expected from the previous results from Lee *et al.*, since BTA **1** is soluble in DMSO and assembly occurs when > 17% H_2O is added. This might be due to poor solubility of the BTA in the 1% DMSO mixture. The solutions were filtered before DLS measurements, to remove dust from the samples. The amount of BTA could possibly be lowered too, by the filtering. In THF, however, no correlation was observed indicating that no aggregates were present, showing that BTA **1** is molecularly dissolved in this solvent. Furthermore, the mean scatter intensity is hundred times higher in the DMSO-H_2O mixtures compared to THF, which is consistent with a higher average mass. This also shows that aggregates are formed in DMSO-H_2O mixtures. We tried to see whether we could see disruption of the aggregates after irradiating the molecules with UV light. However, DLS makes use of a laser in the visible light regime and therefore will lead to isomerization from the *cis* state back to *trans*. Therefore, it is possible that the disruption of the aggregates is not measurable by this technique.

3.4 Investigating the isomerization of the asymmetric light responsive BTA 2

The UV-Vis experiments in the previous paragraph have demonstrated that *cis-trans* isomerization of BTA **1** occurs. In order to improve the solubility of the light responsive BTA, two bulky azobenzene containing side chains were replaced by alkyl chains. The influence of this replacement on the isomerization behaviour had to be investigated. Asymmetric BTA **2** was synthesized containing only one azo group and having an amine group next to the azobenzene (see Figure 3.3). This BTA **2** was also investigated by UV-Vis to study whether isomerization still takes place. To examine this, UV-Vis spectra of BTA **2** (17.5 µM) were recorded before and after irradiating the samples with UV light and subsequently with visible light. The measurements were first done in THF since in this solvent the molecules dissolve well and are thus expected to be in the molecular dissolved state. With DLS it was

confirmed that the molecules were indeed molecularly dissolved in THF, since no correlation was observed.

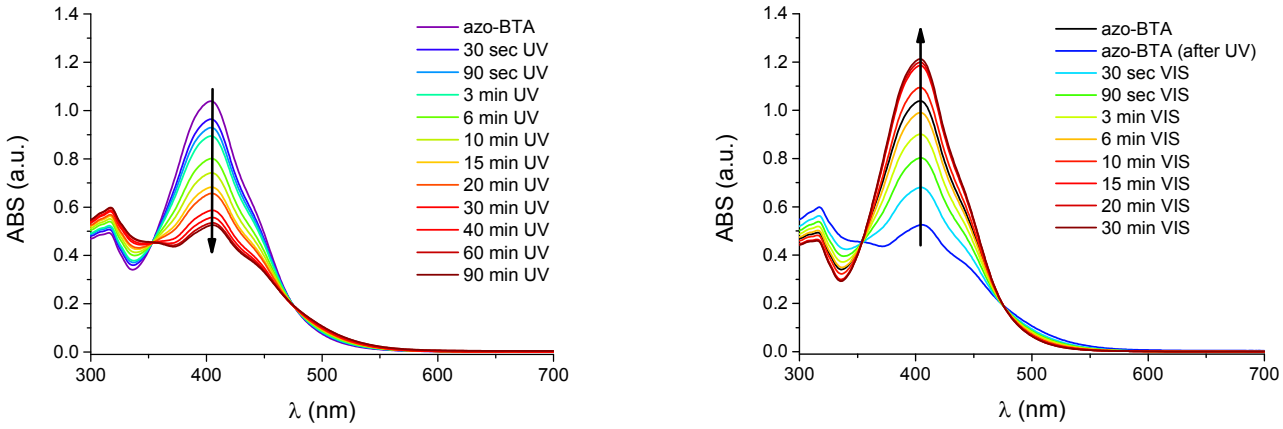

Figure 3.13: UV-Vis spectra of BTA **2** (17.5 µM) in THF upon irradiation with UV-light (375 nm) for various times (left) and subsequent irradiation with visible light (525 nm) for various times (right).

BTA **2** in THF was irradiated with UV light (wavelength: 375 nm). The UV-Vis spectra were measured after various times, in order to investigate the kinetics of the isomerization reaction. The absorption spectra of BTA **2** were shifted toward higher wavelengths compared to the spectrum of BTA **1**. This is a result of the electron donating amine at the para position of the aromatic ring connected to the azo-functionality. As shown in Figure 3.13 the irradiation of BTA **2** with UV light leads to a distinct decrease of the peak at 404 nm, corresponding with the *trans* state of the molecule. No increase of a peak at higher wavelength accompanies this decrease of the *trans* peak, so no peak can be assigned to represent the *cis* state. The isosbestic points in the curves show that there is an equilibrium between two states. Possibly, the peak corresponding with the *cis* state, lies under the peak of the *trans* and is not noticeable since it is weak. After 40 minutes of irradiation, the isomerization is almost complete as can be seen in Figure 3.13.
When the sample was irradiated with visible light (wavelength: 525 nm), in order to switch back to the *trans* state, an increase of the peak at 404 nm is seen. After about 6 minutes the peak belonging to the *trans* state is back in its starting position, corresponding with the thermal equilibrium. When the sample is longer exposed to visible light, the increase of the peak continues and reaches its maximum after about 15 minutes. This maximum lies higher than the starting point from which the experiments started. Showing that in the equilibrium state the molecule is already partly in the *cis* state as expected, since UV light is also present in "normal" light.

In Figure 3.14 the maximum absorption at 404 nm is plotted against the irradiation time to show the kinetic profile of the isomerization from *trans* to *cis* and *cis* to *trans,* respectively. From these results a half-life time was estimated (see experimental section for more details); 10 min for *trans* to *cis* isomerization and 2.5 min for *cis* to *trans*. So the isomerization from *trans* to *cis* is slower in comparison with isomerization from *cis* to *trans*. This is as expected since the *trans* state is more stable.

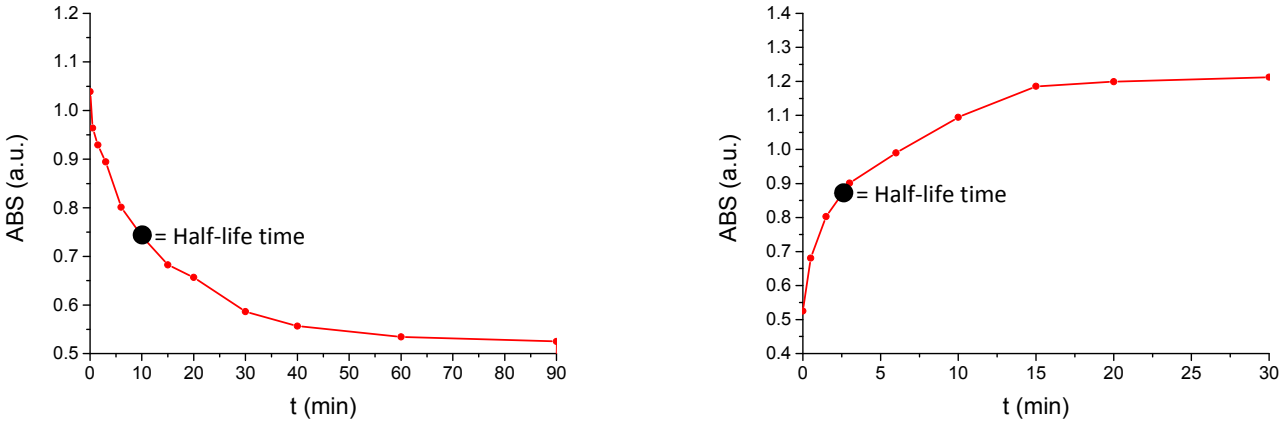

Figure 3.14: Kinetic profile of the isomerization from *trans* to *cis* **2** upon irradiation with UV light (left), and from *cis* to *trans* upon irradiation with visible light (right) UV-Vis data at 404 nm.

In order to evaluate the thermal relaxation of the molecule, **2** was irradiated to bring it to the *cis* state. Then, the solution was stored in dark in order to follow how fast the thermal relaxation was and if it goes back to the original equilibrium. The sample was measured after 16 hours storage in dark, and it was already switched back completely (see Figure 3.15). However, the peak was increased more compared to the equilibrium position and even more than the situation after irradiation with visible light. Of course in the normal equilibrium we have to take into account that UV-light is present in light. Therefore, it might be that a larger percentage is in *cis* state in this situation compared to the situation after dark storage. To our surprise we end up with more molecules in *trans* state compared to the situation after active isomerization to *trans*, for 30 minutes, using visible light. The reason for this behaviour is not understood so far.

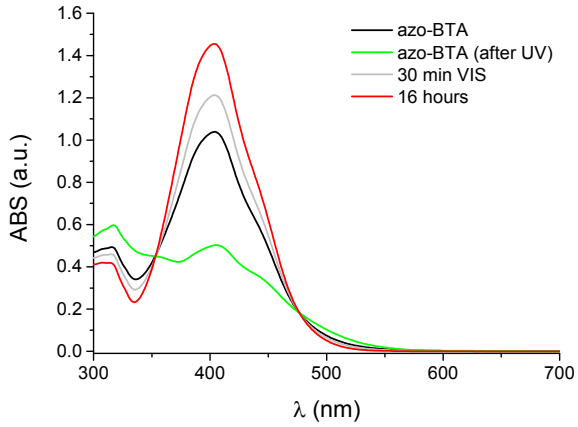

Figure 3.15: UV-Vis spectra of BTA **2** (17.5 µM) in THF before (black) and after irradiation (green) with UV-light (375 nm) and after subsequent 16 hours thermal relaxation (red) or irradiation (grey) with visible light (525 nm).

We also wanted to investigate the behaviour of BTA **2** in assembled state. Therefore, a solvent was required in which self-assembly of **2** occurs. In contrast to many other BTAs, BTA **2** was not soluble in solvents such as methylcyclohexane and water, and was too soluble in acetonitrile. In contrast, in toluene BTA **2** dissolves after sonication and heating of the sample and precipitation only takes place

after a few days. Indicating that the molecule might be in the assembled state in this solvent. No measurements in DMSO-H_2O mixtures were done, since the solubility of BTA **2** was improved compared to BTA **1**, to become able to dissolve the molecule in other solvents.
Since BTA assembly gets disrupted when samples are heated and this gives a red shift in the UV-Vis spectrum. The spectra at different temperatures were measured, in toluene, cooling down from 90 °C to 20 °C. From the spectra from the cooling experiment a red shift can be observed when the sample is cooled down (Figure 3.16). This suggests that BTA **2** self assembles in toluene. BTAs have shown a shift in previous studies as well, when a sample was cooled down, however, in those cases a blue shift was seen.[9] This blue shift is caused by the amides that tilt out of the plane when the H-bonds are formed. In BTA **2** the peak is derived from the azo-bond indicating better ordering upon the temperature change.

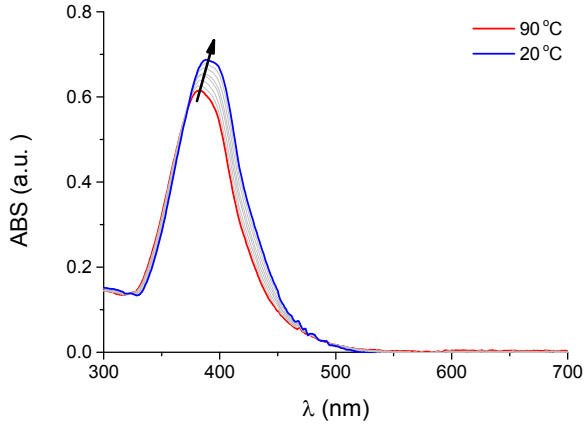

Figure 3.16: Temperature-dependent UV-Vis spectra of BTA **2** (17.5 µ) in toluene cooling from 90 to 20 °C.

To investigate the switching behaviour of BTA **2** in assembled state the UV-Vis spectra were recorded before and after irradiating the samples with UV light and subsequently by visible light. Again the UV-Vis spectra were recorded after various irradiation times to be able to compare the kinetics with the measurements in THF. As shown in Figure 3.17 the spectrum of BTA **2** is similar as before with a maximum absorption at 388 nm compared to the 404 nm in THF, due to the different polarity of the solvent. Upon irradiation of the sample with UV light (375 nm) the peak decreases and no new peak appears, corresponding with the results in THF. So isomerization from the *trans* to the *cis* state can be observed, in both THF and toluene, in a similar fashion. After 30 minutes of irradiation the isomerization is almost complete as can be seen in Figure 3.17.

The peak at 388 nm increases when the sample is irradiated with visible light (525 nm). This time the isomerization from *cis* to *trans* state is going much slower, after one hour of irradiation the *trans* state peak is still not back at the original intensity (see Figure 3.17).

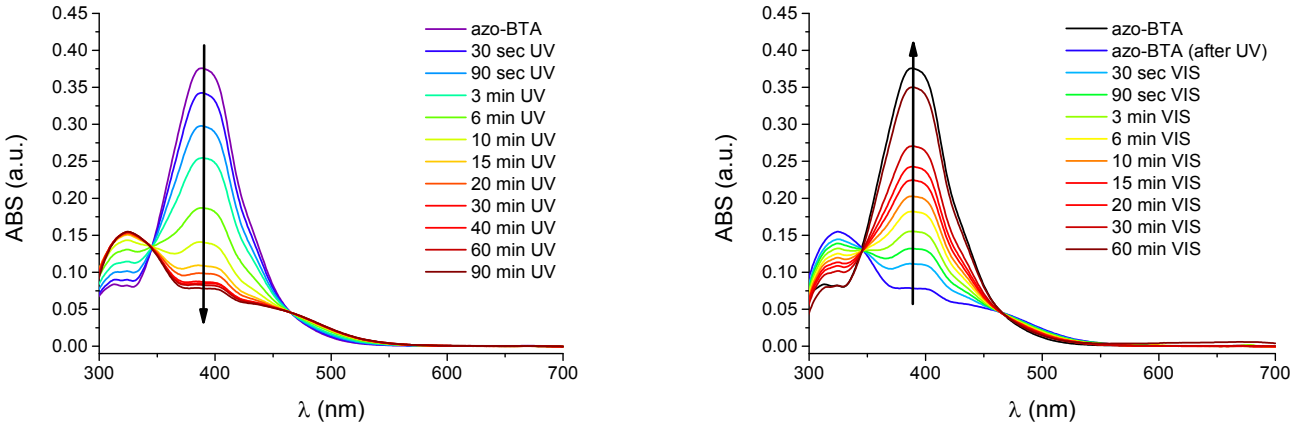

Figure 3.17: UV-Vis spectra of BTA **2** (17.5 µM) in toluene upon irradiation with UV-light (375 nm) for various times (left) and subsequent irradiation with visible light (525 nm) for various times (right).

The maximum absorption at 388 nm is plotted versus the irradiation time to see the kinetic profile of the isomerization from *trans* to *cis* and *cis* to *trans* in toluene (see Figure 3.18). From these results a half-life time could be estimated (see experimental section for more details); 4 min for *trans* to *cis* isomerization and 15 min for *cis* to *trans*. Showing that isomerization from *trans* to *cis* is faster in comparison to the isomerization from *cis* to *trans,* this is opposite to the measurements in THF. This difference might be induced by the effect of the aggregation on the isomerization process.

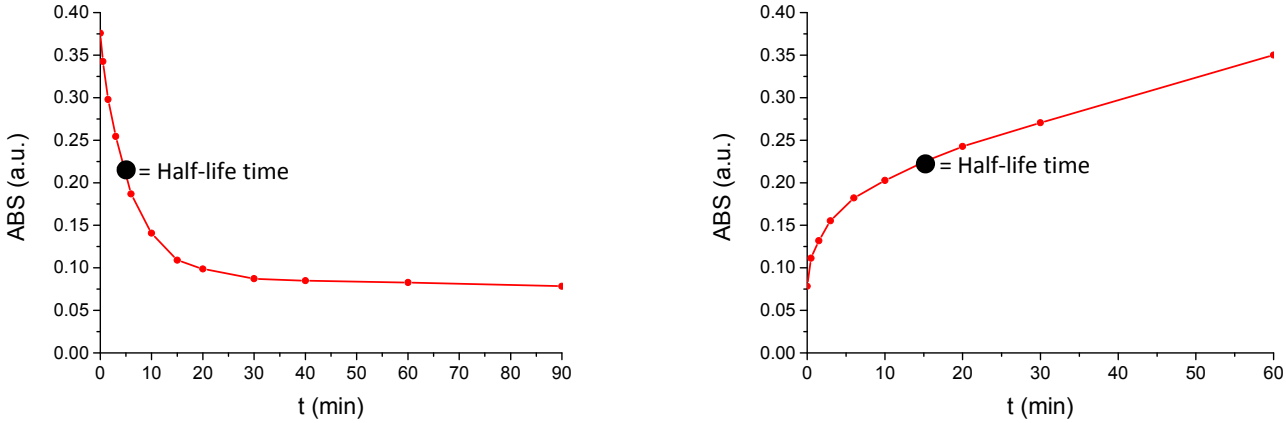

Figure 3.18: Kinetic profile of the isomerization in toluene from *trans* to *cis* **2** upon irradiation with UV light (left), and from *cis* to *trans* upon irradiation with visible light (right) UV-Vis data at 388 nm.

In order to confirm that the BTA is in assembled state in toluene circular dichroism spectroscopy (CD) is used. This is not straight forward as, the typical Cotton effect of the BTA aggregation that is related to the amide packing lies around 200 nm and the solvent absorption of toluene coincides with that region. However, due to the BTA aggregation the azo-compounds are also stacked in that situation which might result in a Cotton effect around 350-400 nm. This effect is observed in the CD spectra of BTA **2** in toluene as shown in Figure 3.19, the effect, however, is only one mdeg and thus very small. When the molecule is irradiated with UV light this Cotton effect disappears. This indicates

that the packing of the azo-compounds is lost upon irradiation. This is expected when the azo-bond isomerizes from *trans* to *cis*, since the conformational change disrupts the ordering. When the sample was irradiated with visible light, no reappearance of the Cotton effect was seen.

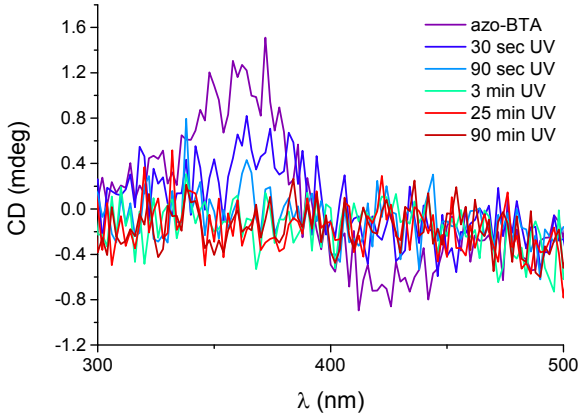

Figure 3.19: CD spectra of **2** (17.5 µM) in toluene, showing disappearance of the Cotton effect when the sample is irradiated with UV light.

To show that aggregation of **2** occurs in toluene and no aggregation takes place in THF, IR was used to investigate whether hydrogen-bonding takes place in these solvents. This can be determined by checking if the characteristic peak of the intermolecular hydrogen bonding, 3240 cm^{-1}, is seen in the IR spectrum.[8]

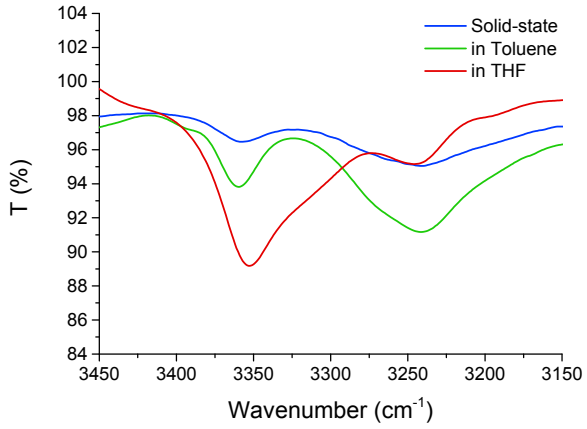

Figure 3.20: IR spectra of BTA **2** in solid state, and at a concentration of 0.5 mM in toluene and THF.

As can be seen in Figure 3.20 in toluene the characteristic peak for intermolecular hydrogen bonding is present (3241 cm^{-1}). In THF this peak is less pronounced indicating that less or no aggregation finds place in this solvent as already observed using DLS. The presence of the Cotton effect and the H-bonding peak shows that BTA **2** forms aggregates in toluene.

3.5 Conclusion

The aim of this chapter was to investigate the isomerization of light-responsive BTAs and the effect of the isomerization on the aggregation of the BTAs. Irradiation of BTA **1**, with three light-responsive arms, with UV-light leads to isomerization from *trans* to *cis* state of the molecule as was shown using UV-Vis spectroscopy. Isomerization to *cis* state is observed when the sample is irradiated with visible light, these measurements were done in THF and 50% DMSO-H_2O. With DLS we confirmed that the BTA is molecularly dissolved in THF and self-assembled in DMSO-H_2O.

For BTA **2**, with only one light-responsive arm, irradiation experiments with UV and subsequently visible light were done in THF as well as toluene, and the kinetic profile of the isomerization was investigated. From the UV-Vis data of the irradiation of BTA **2** a clear decrease of the peak at 404/388 nm (depending on the solvent) was observed. An increase of the peak corresponding to the *cis* state was not seen, possibly this peak falls under the (residual) *trans* peak. Upon irradiation with visible light the molecule isomerizes back to the *trans* state in THF. The amount of molecules in *trans* state is higher after irradiation with visible light since in the equilibrium state the molecule is not active isomerized to this *trans* state. From the kinetic profiles of the isomerization in THF and toluene half-life times for the transformation from *trans* to *cis* are found to be 10 and 4 minutes, respectively. For the isomerization back from *cis* to *trans* the half-life times in THF and toluene are found to be 2.5 and 15 minutes, respectively.

The aggregation of BTA **2** in toluene was indicated by the shift of the absorption peak upon changes in the temperature of the sample. This was confirmed looking at the H-bonding peak at 3240 cm^{-1} with IR spectroscopy that is present for the molecule in toluene and is not observed in THF. Also a small Cotton effect was seen with CD spectroscopy indicating an ordered fashion of the molecules in solution. The Cotton effect disappears when the molecule is irradiated with UV light as expected since the molecule undergoes a conformational change, which makes aggregation more difficult according to literature.

Also in the solid state with IR the typical H-bonding peak is observed, when the molecule is heated up to 180 °C this peak starts to shift and decrease. And at 210 °C the H-bonding is disrupted completely, this is corresponding with the DSC data which gives a melting temperature of 188 °C. With POM it is possible to see that the molecule shows birefringence and this disappears around 190-200°C also confirming the melting around this temperature. When the sample was allowed to cool down again the birefringence reappeared and when pressure was applied a flow of the birefringence was observed without destroying the crystals, this indicates liquid crystalline behaviour. However, using wide angle X-ray scattering is was not possible to establish that the material is liquid crystalline since peaks come-up upon heating the sample which indicate crystallinity and these peaks disappear again at 190 °C in agreement with the melting temperature of the material. From the WAXS data, columnar hexagonal packing of BTA stacks with an interdiscotic distance of 3.54 Å was determined which is in agreement with the morphology from measurements on other BTAs.

It is possible to conclude that both BTA **1** and **2** are able to isomerize from their stable *trans* state to the metastable *cis* state making use of UV-light and back to the *trans* state with light in the visible range. The adjustment from BTA **1** to **2** makes the molecule better soluble but the molecule still doesn't dissolve in solvents such as methylcyclohexane, which would be convenient in order to do

CD measurements and be able to determine the aggregation better. However, when the molecule would be attached to silica beads the solubility will depend for the largest part on the silica beads and therefore the problem might be solved after the coupling of BTA **2** to beads.

3.6 Experimental section

Materials

Chemicals and solvents were used as received unless specified otherwise. Solvents were obtained from Sigma-Aldrich in spectroscopic grade.

CD measurements

Circular dichroism spectra were recorded on a Jasco J-815 spectrapolarimeter equipped with a PFD-425s/15 Peltier-type temperature controller with a temperature range of -10 °C to 110°C. Sensitivity, time constant and scan rate were chosen appropriately. Experiments were performed in a 1 cm Hellma quartz cell.

IR measurements

Infrared spectra were recorded using a Perkin Elmer Spectrum Two FT-IR spectrometer equipped with a Perkin Elmer Universal ATR Two Accessory. A 1.0 mm CaF Cell was used for the IR measurements in solution.
Temperature-dependent IR was recorded with a Bruker Optics Tensor 27 FTIR spectrometer, equipped with a temperature controller Pike GladiATR EZ-ZONE PM.

UV-Vis measurements

UV-Vis experiments were performed on a Jasco V-650 spectrophotometer equipped with a JASCO ETCR-762 temperature controller. The measurements were done with a scan-speed of 100 nm/min, a data pitch of 1.0 nm, a bandwidth of 1.0 nm, over a wavelength range from 700 to 220 nm. Experiments were performed in a 1 cm Hellma quartz cell.

WAXS measurements

Wide angle X-ray scattering experiments were performed on a SAXSLAB Ganesha system using a GeniX-Cu ultra-low divergence source producing X-ray photons (wavelength of 1.54 Å and a flux of 1 x 10E8 ph s^{-1}). Scattering patterns were collected using a Pilatus 300K silicon pixel detector 487x619 pixels on 172 μm^2 and the sample-to-detector distance was 81 mm.

Dynamic light scattering measurements

DLS experiments were conducted on an ALV/CG-3 MD-4 compact goniometer system equipped with a Multiple Tau digital real time correlator (ALV-7004) and a solid state laser (λ = 532 nm; 40 mW). Experiments were done for angles from 30 to 150°, averaging over 3 x 50 s runs at a temperature of 25°C. Samples were filtered over a 0.45 µm PTFE filter.

Polarized optical microscopy

POM measurements were done using a Jenaval polarization microscope equipped with a Linkam THMS 600 heating device, with crossed polarizers.

Differential scanning calorimetry

The transitions were determined using a PerkinElmer Pyris 1 DSC under a nitrogen atmosphere with heating and cooling rates of 10 K min^{-1}.

Methods

The half-life time was determined by subtracting the lower intensity value (at start or plateau) from the high intensity, and dividing this value by two gave the intensity corresponding with the half-life time.

The BTAs were dissolved in THF, toluene or DMSO at a 10 times higher concentration adjusted for the concentration change after addition of water in case of the DMSO-H_2O sample. These stock solutions were heated and sonicated before taking the correct amount of material and diluting it by adding solvent(s). The samples were heated and sonicated once more before measuring them after cooling down.

Irradiation of the azo BTA **2** was done using the CD apparatus at the appropriate wavelength (UV: 375 nm, vis: 525 nm) with a minimum bandwidth (15 nm) during the appropriate time length. The experiments were performed in 1 cm Hellma quartz cell.

3.7 References

1. S. Lee, S. Oh, J. Lee, Y. Malpani, Y.-S. Jung, B. Kang, J. Y. Lee, K. Ozasa, T. Isoshima, S. Y. Lee, M. Hara, D. Hashizume and J.-M. Kim, *Langmuir*, 2013, **29**, 5869-5877.
2. N. Tamaoki, *Adv. Mater.*, 2001, **13**, 1135-1147.
3. S. Pieraccini, S. Masiero, G. P. Spada and G. Gottarelli, *Chem. Commun.*, 2003, 598-599.
4. K. Katayama, Y. Choi, J. W. Kang, Z. Yaqoob, P. T. C. So, T. Fujii, S. Kuwahara, K. Takado and T. Ikeda, *Phys. Chem. Chem. Phys.*, 2014, **16**, 27074-27077.
5. C. L. van Oosten, C. W. M. Bastiaansen and D. J. Broer, *Nat. Mater.*, 2009, **8**, 677-682.
6. T. Mes, M. M. E. Koenigs, V. F. Scalfani, T. S. Bailey, E. W. Meijer and A. R. A. Palmans, *ACS Macro Letters*, 2011, **1**, 105-109.
7. M. García-Iglesias, B. F. M. de Waal, I. de Feijter, A. R. A. Palmans and E. W. Meijer, *Chem.-Eur. J.*, 2015, **21**, 377-385.
8. P. J. M. Stals, M. M. J. Smulders, R. Martín-Rapún, A. R. A. Palmans and E. W. Meijer, *Chem.-Eur. J.*, 2009, **15**, 2071-2080.
9. S. Cantekin, T. F. A. de Greef and A. R. A. Palmans, *Chem. Soc. Rev.*, 2012, **41**, 6125-6137.

Chapter 4: Orthogonal self-assembly

4.1 Introduction

In this chapter, we study the orthogonal self-assembly of two supramolecular binding motifs. Orthogonal self-assembly means "the independent formation of two different supramolecular structures, each with their own characteristics that coexist within a single system".[1] By combining orthogonal binding motifs, materials can be formed in which it is possible to control the material properties via both interactions gaining more control over these properties. This gives opportunities to control the complexity and hierarchical order to a greater extent in comparison to a system in which only one binding motif is used. In addition the use of two different building blocks in a material leads to combined properties to the formed material.
A simple example of orthogonal self-assembly is that seen in DNA bases in which thymidine only forms a pair with adenine and guanine with cytosine. These base pairs assemble without interfering with the other base pairs, and the system can be extended with more supramolecular motifs shown by Sismour *et al*.[2] This example also shows the importance of orthogonal binding motifs for information storage, since this is not possible without the use of two orthogonal binding motifs.

A recent covalent example of the use of two orthogonal structures is that of block copolymers. Using two orthogonal hydrogen bonding moieties at the chain-ends, a triblock copolymer was made using a one-pot synthesis.[3] Block copolymers are used as building blocks for various functional nanostructured materials, such as electronic devices and drug delivery because of their tunable phase separation behaviour.[4] Another interesting example is that of dendrimers. The use of two (or more) orthogonal binding motifs facilitates the construction of highly ordered, layered, dendrimers.[5] Also various complementary hydrogen binding motifs are studied, using a polymer backbone decorated with two different functionalized side chains (based on cyanuric and thymine acid).[6] The cross-links form via orthogonal self-assembly, showing self-sorting in a competitive environment. An example with benzene-1,3,5-tricarboxamide (BTA) is found in a study where it is used as orthogonal supramolecular binding motif in combination with 2-ureido-4[1H]-pyrimidinone (UPy). BTA and UPy functionalized polymers were made, these formed phase separated nanorods in an orthogonal fashion.[7] By introducing an amount of compatibilizer the material properties transform from a sticky viscous liquid to an elastomeric material. So this shows that by the use of two orthogonal binding moieties the material properties can be controlled to greater extent.

In this chapter we use the BTA based supramolecular binding motifs **2** because these are well studied, making the use of two orthogonal binding motifs based on these structures interesting. BTA **2** (see Figure 4.1) and a variant with an extended core; oligo(phenylene ethynylene) tricarboxamide (OPE-TA) (**1**), have both been studied extensively and were found to assemble into columnar aggregates.[8, 9] The presence of a stereogenic methyl group in the alkyl side chains provides a preferred helical arrangement of the BTAs and OPE-TAs, resulting in a Cotton effect in CD. Therefore, the self-assembly of the BTA and OPE-TA were studied by circular dichroism (CD) additional to ultraviolet-visible (UV-Vis) spectroscopy.[7,10]

To create dynamic materials that can be controlled via the interactions of the binding motifs, it is useful to fuse these self-assembling supramolecular motifs with large building blocks such as colloids. The use of the two above mentioned supramolecular binding motifs can be useful for this purpose, we aim to create a system in which the two motifs only self-assemble with the same binding motifs, thus creating two different phases. However, to create such a system the binding motifs have to be orthogonal. Therefore, the extent to which benzene-1,3,5-tricarboxamide (BTA) and oligo(phenylene ethynylene) tricarboxamide (OPE-TA) self-assemble orthogonally was examined by CD and UV-Vis spectroscopy.

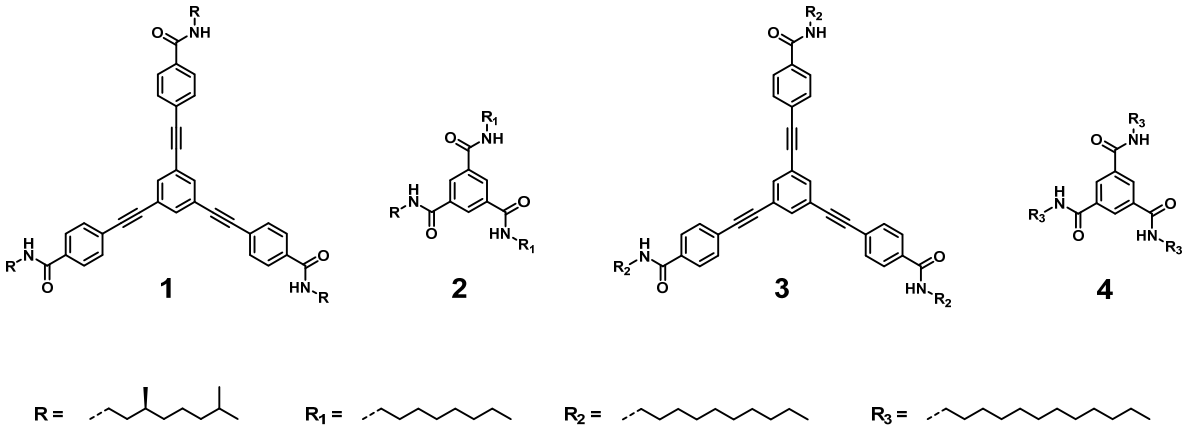

Figure 4.1: Structures of chiral OPE-TA **1** and BTA **2**, and achiral OPE-TA **3** and BTA **4**.

4.2 Investigating the orthogonality in self-assembly of the BTA and OPE-TA

The influence of both supramolecular motifs on each other's self-assembly behaviour was evaluated by CD and UV-Vis spectroscopy. Cooling curves of the chiral molecules were obtained with and without the achiral OPE-TA **3** and the achiral BTA **4**, respectively, to see whether there were differences in the behaviour of the chiral motifs due to the presence of the analogue. The analogues used are achiral molecules to avoid measuring a mixed CD signal of the two individual CD effects of the BTA and OPE-TA. Moreover, the measurements were done for the chiral BTA as well as the OPE-TA to see whether neither of them influenced the other. By comparing the CD effects, the influence of the two binding motifs on each other can be determined. Temperature-dependent measurements were performed by heating the samples to a temperature above the critical temperature of elongation (T_e). The T_e was determined by slowly cooling down the samples until the CD effect reemerged. When neither the spectra nor the T_e are influenced by the presence of the analogues, these do not interfere with the assembly of the chiral motifs, and thus the binding motifs are considered orthogonal.

The CD spectra, UV-Vis spectra, and cooling curve of the (*S*)-BTA **2** were obtained as reference. The self-assembly of the (*S*)-BTA **2** (c = 16 µM) gives a Cotton effect at 225 nm and a λ_{max} of 209 nm in methylcylohexane (MCH) (see Figure 2 a and b). Cooling curves in CD and UV (λ = 225 nm), show a

T_e at 55 ° (see Figure 4.3). If these measurements done in the presence of the achiral OPE-TA **3**, would result in a lowering of the T_e it would mean that the formed aggregates are less stable due to the influence of the OPE-TA.

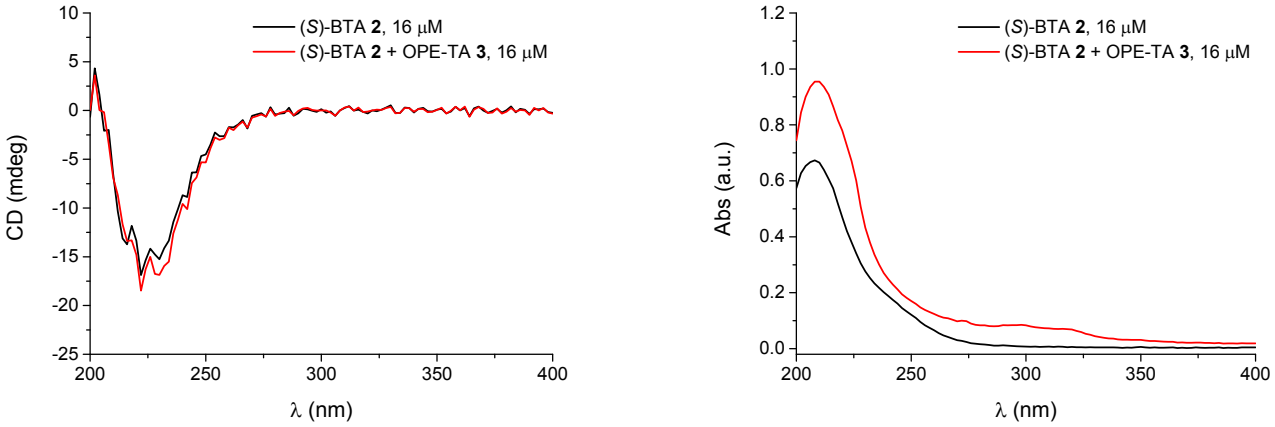

Figure 4.2: a) CD spectra of BTA **2** c = 16 µM in MCH in the absence in black and the presence of OPE-TA **3** c = 16 µM in red at 20 °C (c_{tot} = 32 µM). b) UV-Vis spectra of BTA **2** c = 16 µM in MCH in the absence in black and the presence of OPE-TA **3** c = 16 µM in red at 20 °C (c_{tot} = 32 µM).

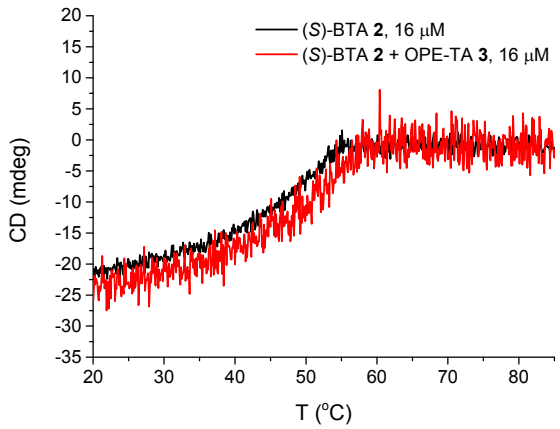

Figure 4.3: Temperature-dependent CD measurement of BTA **2** c = 16 µM at λ = 225 nm in MCH in black and in the presence of OPE-TA **3** c = 16 µM in red (c_{tot} = 32 µM).

Figure 4.2 shows that the Cotton effect of the (*S*)-BTA **2** is not significantly influenced by the presence of the OPE-TA. If they would co-assemble an increase in the CD effect would be expected, due to the sergeant-soldiers principle; the chiral "sergeant" would introduce a strong preference of handedness into the stacks containing the achiral "soldiers" amplifying the CD effect.[11, 8] In the samples with the achiral OPE-TA **3** at temperatures below 40 °C some solubility problems for the achiral OPE-TA were seen. This can be observed in the UV-Vis spectrum in Figure 4.2b by the low absorption of the OPE-TA (260-340 nm), compared to the absorption of the BTA (200-240 nm) at the same concentration. The temperature curves of (*S*)-BTA show a T_e of approximately 55 °C and a T_e of

roughly 58 °C when the OPE-TA was added to the samples. The CD effect after addition of the OPE-TA was slightly changed but this is within the experimental uncertainty due to the high absorption in sample at the used wavelength by both the BTA and the OPE-TA. These results show that the OPE-TA does not significantly interfere with the BTA aggregation, as is required for an orthogonal system.

To investigate if vice versa BTAs have no influence on OPE-TA self-assembly the procedure was repeated with the (*S*)-OPE-TA **1**. The self-assembly of the (*S*)-OPE-TA **1** (c = 16 µM) results in a Cotton effect at 280, 304 and 324 nm and a λ_{max} at 220 and 294 nm (see Figure 4.4 a and b) in methylcylohexane (MCH). These measurements were repeated in the presence of the achiral BTA **4** (c = 16 µM) to see whether there is influence in the presence of the BTA. Figure 4 shows that there is no influence on the Cotton effect of the (*S*)-OPE-TA **1** due to addition of the BTA to the sample. Also temperature-dependent CD and UV-Vis measurements were done (λ = 304 nm) (see Figure 4.5). In the temperature curves of the (*S*)-OPE-TA **1**, a T_e of roughly 68 °C is observed without the BTA and a T_e of 67 °C when the BTA **4** is present in the sample. The CD effect, however, is again lower in presence of the achiral compound, indicating a small decrease in OPE-TA stacking in the presence of the BTA. These results for the OPE-TA show that there is no significant change in the CD and UV-Vis spectra and also not in the T_e upon addition of the achiral BTA **4**, so the BTA has no significant influence on the self-assembly of the OPE-TA, as was required in order to be able to use them as orthogonal binding moieties.

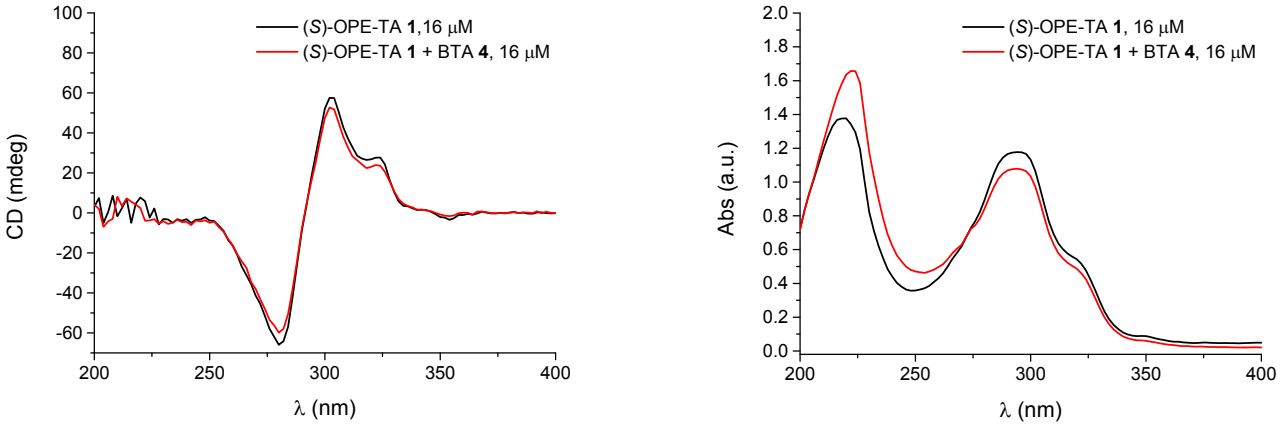

Figure 4.4: a) CD spectra of OPE-TA **1** c = 16 µM in MCH in the absence in black and the presence of BTA **4** c = 16 µM in red at 20 °C (c_{tot} = 32 µM). b) UV-Vis spectra of OPE-TA **1** c = 16 µM in MCH in the absence in black and the presence of BTA **4** c = 16 µM in red at 20 °C (c_{tot} = 32 µM).

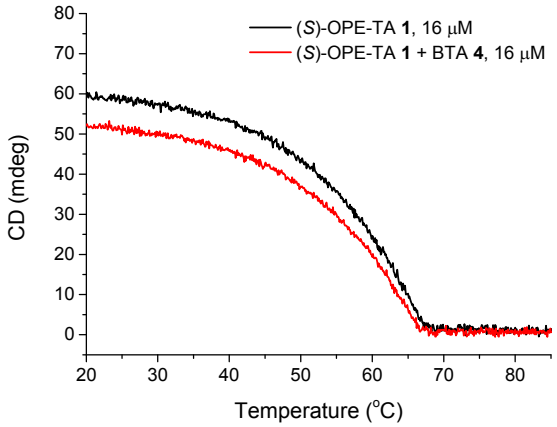

Figure 4.5: Temperature-dependent CD measurement of OPE-TA **1** c = 16 µM at λ = 304 nm in MCH in black and in the presence of BTA **4** c = 16 µM in red (c_{tot} = 32 µM).

Eventually, the above discussed supramolecular motifs will be coupled to surface modified silica beads. Measurements on these beads are often done in cyclohexane. Therefore, we investigated whether the orthogonal self-assembly observed in methylcyclohexane is also obtained in cyclohexane. Similarly as described before, CD spectra, UV-Vis spectra and cooling curves were recorded in cyclohexane of the OPE-TA before and after addition of the BTA analogue.

The self-assembly of the (*S*)-OPE-TA in cyclohexane gives the same Cotton effect and λ_{max} as observed in MCH (see Figure 4.6 a and b).

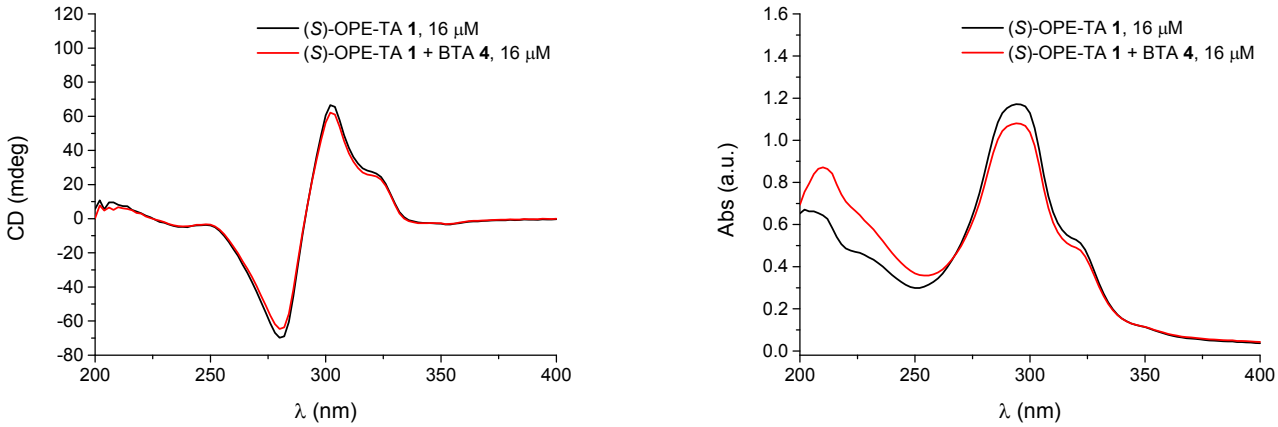

Figure 4.6: a) CD spectra of OPE-TA **1** c = 16 µM in CH in the absence in black and the presence of BTA **4** c = 16 µM in red at 20 °C (c_{tot} = 32 µM). b) UV spectra of OPE-TA **1** c = 16 µM in CH in the absence in black and the presence of BTA **4** c = 16 µM in red at 20 °C (c_{tot} = 32 µM).

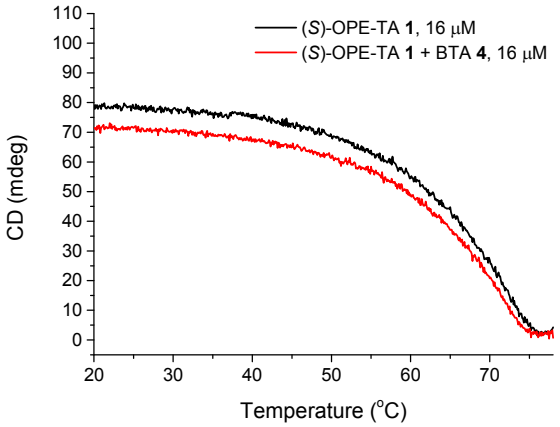

Figure 4.7: Temperature-dependent CD measurement of OPE-TA **1** c = 16 μM at λ = 304 nm in CH in black and in the presence of BTA **4** c = 16 μM in red (c_{tot} = 32 μM).

Figure 4.7 shows the Cotton effect of the (*S*)-OPE-TA **3** with and without the BTA **4**, no change upon addition of the BTA is seen. A T_e of approximately 76 °C without the BTA **4** and of roughly 75 °C are observed in the presence of the BTA. Again a lowering of the CD effect is observed when the achiral compound is present in the sample, indicating a small decrease in OPE-TA assembly in presence of the BTA. The results of the measurements in CH show that the BTA interferes not significantly with the assembly of the OPE-TA in cyclohexane as well, the orthogonality seen in MCH holds in CH, making it possible to use these binding moieties coupled to the mentioned beads for orthogonal self-assembly.

4.3 Conclusion

The aim of this chapter was to determine to what extent the BTA and OPE-TA are orthogonal binding moieties. Therefore, the CD and UV-Vis spectra of the chiral BTA and OPE-TA were measured with and without the achiral OPE-TA or BTA analogues. Also temperature-dependent measurements were done to determine the T_e of the BTA and OPE-TA in absence and presence of the analogues. The CD and UV-Vis spectra show that the self-assembly of the BTA and OPE-TA is hardly influenced by the presence of the other binding motif, the temperature-dependent measurements also show no significant change of the T_e upon addition of the analogue for both the cases. The presence of the BTA does, however, lower the amount of OPE-TA that assembles in reference to the situation without the BTA. A smaller influence of the BTA on the OPE-TA is seen for the OPE-TA upon the addition of the BTA. The measurements in MCH are comparable to those in CH showing that the orthogonality also holds in this solvent. To summarize, these results show that the BTA and OPE-TA do not significantly influence each other. So the BTA and OPE-TA can be used as orthogonal binding moieties grafted onto beads in further research.

4.4 Experimental section

Materials

Chemicals and solvents were used as received unless specified otherwise. Solvents were obtained from Sigma-Aldrich in spectroscopic grade. Compound **1** and **3** were synthesized by Fátima García-deMelo described in reference 10 and compound **2** and **4** were synthesized by Bas de Waal as described in references 12 and 13.

CD and UV-Vis measurements

Circular dichroism and ultraviolet-visible spectra were recorded on a Jasco J-815 spectropolarimeter equipped with a PFD-425s/15 Peltier-type temperature controller with a temperature range of -10 °C to 110°C. Sensitivity, time constant and scan rate were chosen appropriately. Experiments were performed in a 1 cm Hellma quartz cell.

Methods

The samples of the BTA and OPE-TA for the CD measurements were prepared by dissolving the BTA/OPE-TA in MCH or CH in a 10x more concentrated fashion. Dissolving of the molecules was achieved using ultra sonication and heating of the samples. After 30 minutes sonication of the stock solution at 40 °C the required amount was taken from the stock solution and diluted. Measurements were done after 15 minutes of sonication of the samples.

4.5 References

1. A. Heeres, C. van der Pol, M. Stuart, A. Friggeri, B. L. Feringa and J. van Esch, *J. Am. Chem. Soc.*, 2003, **125**, 14252-14253.
2. A. M. Sismour and S. A. Benner, *Expert Opin. Biol. Ther.*, 2005, **5**, 1409-1414.
3. S. K. Yang, A. V. Ambade and M. Weck, *J. Am. Chem. Soc.*, 2010, **132**, 1637-1645.
4. K. Kataoka, A. Harada and Y. Nagasaki, *Adv. Drug Delivery Rev.*, 2001, **47**, 113-131.
5. F. Grimm, K. Hartnagel, F. Wessendorf and A. Hirsch, *Chem. Commun.*, 2009, 1331-1333.
6. C. Burd and M. Weck, *Macromolecules*, 2005, **38**, 7225-7230.
7. T. Mes, M. M. E. Koenigs, V. F. Scalfani, T. S. Bailey, E. W. Meijer and A. R. A. Palmans, *ACS Macro Letters*, 2011, **1**, 105-109.
8. M. M. J. Smulders, A. P. H. J. Schenning and E. W. Meijer, *J. Am. Chem. Soc.*, 2007, **130**, 606-611.
9. F. García, P. M. Viruela, E. Matesanz, E. Ortí and L. Sánchez, *Chem.-Eur. J.*, 2011, **17**, 7755-7759.
10. F. Garcia, P. A. Korevaar, A. Verlee, E. W. Meijer, A. R. A. Palmans and L. Sanchez, *Chem. Commun.*, 2013, **49**, 8674-8676.
11. L. Brunsfeld, B. G. Lohmeijer, J. J. M. Vekemans and E. W. Meijer, *J. Inclusion Phenom. Macrocyclic Chem.*, 2001, **41**, 61-64.
12. K. Hanabusa, C. Koto, M. Kimura, H. Shirai and A. Kakehi, *Chem. Lett.*, 1997, **26**, 429-430.
13. P. J. M. Stals, M. M. J. Smulders, R. Martín-Rapún, A. R. A. Palmans and E. W. Meijer, *Chem.-Eur. J.*, 2009, **15**, 2071-2080.

Chapter 5: Conclusion and outlook

Symmetrically and asymmetrically substituted light responsive BTAs were successfully synthesized. The synthesis of the asymmetric BTA was more difficult due to fast hydrolysis of the amide bond when a work up in presence of water is done on a larger scale. However, a new synthesis route was designed in a way that no water is required after the formation of the amide bond. For the purification of the asymmetrically substituted BTA **2** we found that trituration is an effective purification method. Column chromatography was less convenient since a low yield was obtained because of hydrolysis of the amide bond. The light acidity of the silica column catalyzes hydrolysis of the amide, between the azo-compound and the BTA core. For this reason a new approach was designed to obtain BTA **2**. This synthetic approach needs more evaluation in further research in order to determine whether this approach is successful and an improvement of the synthetic route discussed here.

With DLS, we observed that both the symmetrically and asymmetrically substituted BTAs are molecularly dissolved in THF and that they self-assemble in a mixture of 50% DMSO−H_2O or toluene for **1** and **2**, respectively. Aggregation of **2** in toluene was also indicated by the shift in its UV spectra upon changes in temperature. In addition aggregation in toluene was indicated, by the presence of the hydrogen bonding peak that was more pronounced in toluene compared to THF. Furthermore, the small Cotton effect present in the CD spectrum of **2**, when it was dissolved in toluene, strengthens this hypothesis.

The switching behaviour of both BTAs was investigated using UV-Vis spectroscopy. For BTA **1** a decrease of the peak belonging to the *trans* state of the molecule was seen upon irradiation with UV light and a small increase of the peak corresponding with the *cis* state of the molecule. Switching back was achieved via thermal relaxation as well as by irradiation with visible light.
Also for BTA **2** isomerization was observed upon irradiation with UV and visible light. For this molecule the kinetics of the isomerization were evaluated in both THF and toluene. Half-life times of 10 and 4 minutes from *trans* to *cis* were measured in THF and toluene, respectively. In addition 2.5 and 15 minutes was found for the isomerization from *cis* to *trans* in THF and toluene, respectively. Furthermore, the small Cotton effect of BTA **2** in toluene disappears upon irradiation with UV light, which indicates the disruption of the self-assembly due to *trans-cis* isomerization.
The presence of hydrogen bonds for BTA **2** in toluene was observed with IR spectroscopy. In THF less or no hydrogen bonding was observed, showing that aggregation takes place in toluene and the molecule is molecularly dissolved in THF, in accordance with the DLS results.

The solid state behaviour of BTA **2** was investigated. Temperature-dependent IR measurements, WAXS, POM and DSC showed a transition around 188 °C. These techniques showed that the material becomes a liquid above this temperature, the hydrogen bonding and thereby ordering of the molecules is lost. The temperature-dependent behaviour is not completely clear so far, making use of the combination of techniques mentioned.

Having the switching and assembly behaviour investigated, the next step is to couple the BTA to silica beads and investigate the self-assembly in this state and the effect of *cis-trans* isomerization on it. On a small scale the coupling of BTA **2** to succinic anhydride already proved successful. When this

reaction is repeated on a larger scale, it may be possible to couple the light responsive BTA to silica beads. If this is accomplished it is possible to evaluate in more detail whether self-assembly of the BTAs gives the opportunity to orchestrate the assembly of these colloids. Furthermore, it would become possible to see what the effect of the isomerization with light has on the BTA assembly. When the system is able to assemble and dissociate upon irradiation with light, it is possible to create the system we aimed for using this BTA (see Figure 5.1).

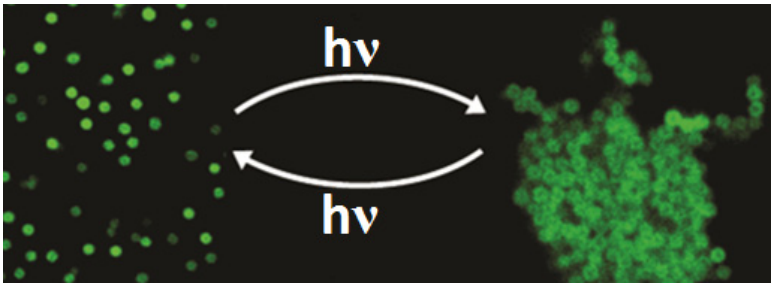

Figure 5.1: Aim: switching between a dissociated and an assembled system of fluorescent colloids using light of different wavelengths.

The orthogonality of the BTA in combination with a second binding motif, in this case the core extended BTA or OPE-TA was evaluated. It was found that the self-assembly of the core extended BTA and the BTA finds place in an orthogonal fashion. The UV and CD spectra of the molecules are hardly influenced by the presence of the analogue. Additionally no significant change in the T_e is seen upon addition of the other binding motif. This shows that orthogonal self-assembly finds place in MCH and CH for these binding moieties and they can be used grafted onto beads as orthogonal binding motifs in further research. Making use of these two orthogonal binding moieties in combination with the isomerization of the azo-bond might give a system in which a self-assembled two-phase system can switch to a random dispersed system of the two molecules (see Figure 5.2).

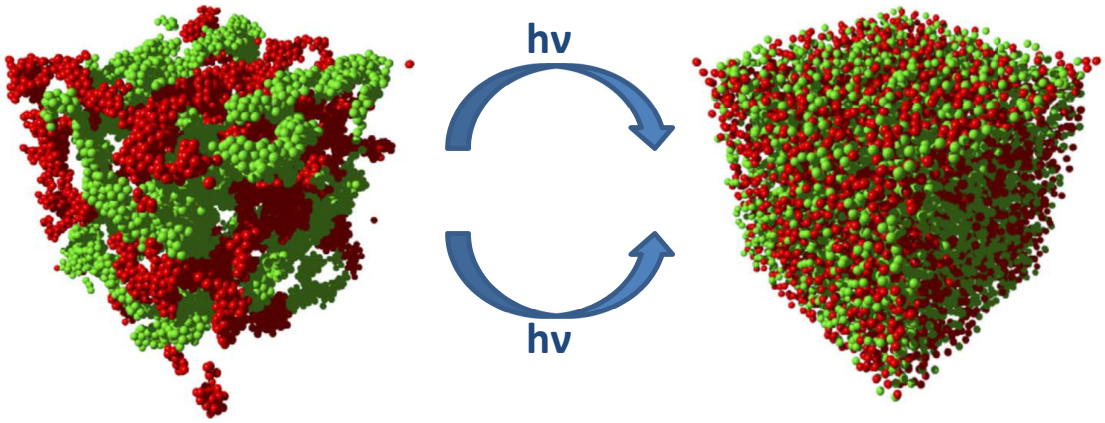

Figure 5.2: Orthogonal binding motifs in self-assembled and dissociated state.

Dankwoord

Het einde van mijn afstudeeronderzoek komt nu inzicht, in het afgelopen jaar heb ik veel geleerd. Daarom is de tijd gekomen, nu alle resultaten in dit verslag staan beschreven, om iedereen die me heeft begeleid, geholpen, of op een andere manier een andere bijdrage heeft geleverd aan dit onderzoek te bedanken.

Allereerst wil ik graag Bert Meijer bedanken voor de mogelijkheid om binnen zijn vakgroep mijn afstudeeronderzoek te kunnen doen. Je betrokkenheid, enthousiasme en tips hebben geholpen tijdens de uitvoering van mijn onderzoek.

Ilja Voets en Anja Palmans, ik wil jullie bedanken voor het project dat onder jullie leiding stond, waar ik met veel plezier aan heb gewerkt. Jullie betrokkenheid bij het project en de input tijdens de gesprekken hebben me erg geholpen bij het onderzoek. Hartelijk dank voor jullie sturing, kennis en soms kritische opmerkingen, ook bedankt dat jullie plaats hebben willen nemen in mijn afstudeercommissie.

Isja de Feijter heel erg bedankt voor alle begeleiding, hulp en de tijd die in het onderzoek hebt gestopt. Ik hoop dat je ondanks de drukte in verband met je promotie fijn met me hebt samengewerkt, ik vond het erg leuk en heb veel van je geleerd. Veel succes met je promotie en met je nieuwe baan in Denemarken.

I would like to thank Michael Debije for being a member of the advising committee.

José Berrocal and Miguel García-Iglesias thanks for all your help with the project and measurements, and your guidance the past months. José also thanks for being a member of my graduation committee.

I would like to thank Ralf Bovee, Joost van Dongen and Xianwen Lou for their assistance with the analysis of my compounds.

Henk Eding, bedankt voor alle koppen koffie, het draaiend houden van de printer en zo veel meer. Hans Damen, bedankt voor het bestellen van de benodigde chemicaliën en lab benodigdheden.

Robin Willems en Berry Bögels dank voor jullie hulp met de WAXS metingen. Rob van der Weegen bedankt voor je hulp met de IR metingen in oplossing.

Jolanda Spiering en Fátima García Melo bedankt voor de BTA en OPE-TAs die ik tijdens mijn onderzoek heb gebruikt.

I would like to thank everyone in the water soluble BTA lunch meetings and the soft matter meetings for all help and suggestions regarding my research. Furthermore, I would like to thank all the members of lab 3 for all their help during the lab work.

Ook wil ik alle (voormalig) kantoorgenootjes van alle locaties waar ik heb gezeten graag bedanken voor de fijne sfeer die er was.

Mijn vrienden wil ik bedanken voor hun interesse en bijdrage aan de gezelligheid en ontspanning afgelopen tijd. De koffiepauzes met onder andere Robin, Ludo en Lieke hebben hier op de universiteit ook een grote bijdrage aan gehad.

Als laatste wil ik graag mijn ouders en overige familieleden bedanken voor hun interesse en steun gedurende mijn studie.